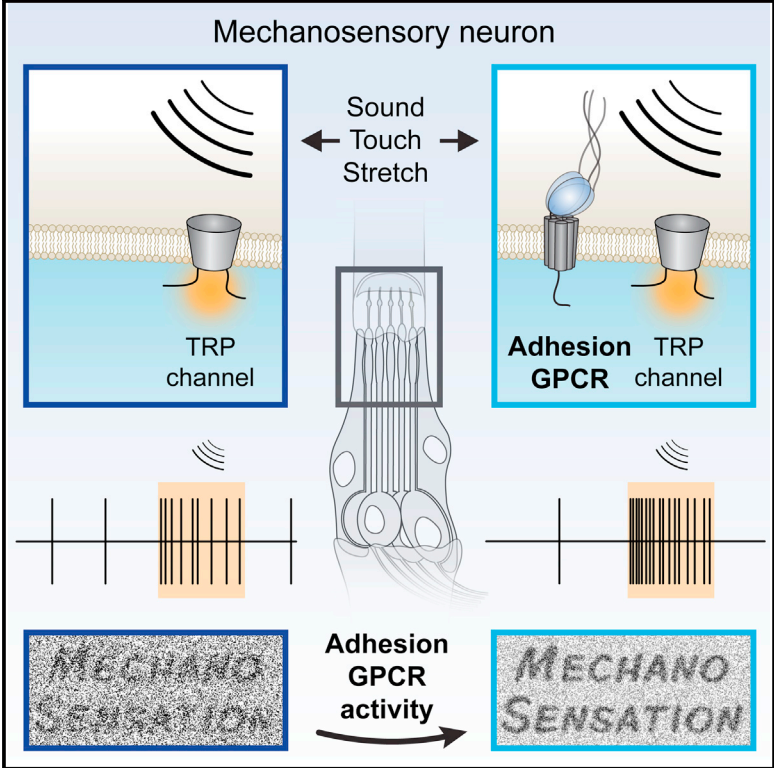


The Adhesion GPCR Latrophilin/CIRL Shapes Mechanosensation

Graphical Abstract



Authors

Nicole Scholz, Jennifer Gehring, ..., Robert J. Kittel, Tobias Langenhan

Correspondence

robert.kittel@uni-wuerzburg.de (R.J.K.), tobias.langenhan@uni-wuerzburg.de (T.L.)

In Brief

The receptive repertoire of adhesion GPCRs has thus far proved elusive. Scholz et al. analyzed a *Drosophila* mutant lacking Latrophilin/CIRL, a prototype member of this receptor class. They establish that the aGPCR Latrophilin/CIRL participates in the recognition of mechanical signals by determining the sensitivity of mechanosensory neurons.

Highlights

- Latrophilin/CIRL is required for mechanosensory neuron function
- Latrophilin/CIRL modulates sensitivity of neuronal mechanosensation
- Latrophilin/CIRL interacts with TRP channels
- In vivo role for a GPCR in mechanosensation is demonstrated

The Adhesion GPCR Latrophilin/CIRL Shapes Mechanosensation

Nicole Scholz,^{1,3} Jennifer Gehring,^{1,3} Chonglin Guan,^{1,3} Dmitrij Ljaschenko,¹ Robin Fischer,^{1,2} Vetrivel Lakshmanan,¹ Robert J. Kittel,^{1,*} and Tobias Langenhan^{1,*}

¹Department of Neurophysiology, Institute of Physiology, University of Würzburg, Röntgenring 9, 97070 Würzburg, Germany

²Department of Neurobiology and Genetics, Biozentrum, University of Würzburg, Am Hubland, 97074 Würzburg, Germany

³Co-first author

*Correspondence: robert.kittel@uni-wuerzburg.de (R.J.K.), tobias.langenhan@uni-wuerzburg.de (T.L.)

<http://dx.doi.org/10.1016/j.celrep.2015.04.008>

This is an open access article under the CC BY-NC-ND license (<http://creativecommons.org/licenses/by-nc-nd/4.0/>).

SUMMARY

G-protein-coupled receptors (GPCRs) are typically regarded as chemosensors that control cellular states in response to soluble extracellular cues. However, the modality of stimuli recognized through adhesion GPCR (aGPCR), the second largest class of the GPCR superfamily, is unresolved. Our study characterizes the *Drosophila* aGPCR *Latrophilin/dCirl*, a prototype member of this enigmatic receptor class. We show that *dCirl* shapes the perception of tactile, proprioceptive, and auditory stimuli through chordotonal neurons, the principal mechanosensors of *Drosophila*. *dCirl* sensitizes these neurons for the detection of mechanical stimulation by amplifying their input-output function. Our results indicate that aGPCR may generally process and modulate the perception of mechanical signals, linking these important stimuli to the sensory canon of the GPCR superfamily.

INTRODUCTION

Because of the nature of their activating agents, G-protein-coupled receptors (GPCRs) are established sensors of chemical compounds (Pierce et al., 2002). The concept that GPCRs may also be fit to detect and transduce physical modalities, i.e., mechanical stimulation, has received minor support thus far. In vitro observations showed that, in addition to classical soluble agonists, mechanical impact such as stretch, osmolarity, and plasma membrane viscosity may alter the metabotropic activity of individual class A GPCR (Chachisvilis et al., 2006; Mederos y Schnitzler et al., 2008; Zou et al., 2004). However, the ratio and relationship between chemical and mechanical sensitivity and the physiological role of the latter remain unclear.

Genetic studies have indicated that adhesion GPCRs (aGPCRs), a large GPCR class with more than 30 mammalian members (Fredriksson and Schiöth, 2005), are essential components in developmental processes (Langenhan et al., 2009). Human mutations in aGPCR loci are notoriously linked to pathological conditions emanating from dysfunction of these underlying

mechanisms, including disorders of the nervous and cardiovascular systems, and neoplasias of all major tissues (Langenhan et al., 2013). However, as the identity of aGPCR stimuli is unclear, it has proven difficult to comprehend how aGPCRs exert physiological control during these processes.

Latrophilins constitute a prototype aGPCR subfamily because of their long evolutionary history. Latrophilins are present in invertebrate and vertebrate animals (Figures 1A and 1B; Fredriksson and Schiöth, 2005), and their receptor architecture has remained highly conserved across this large phylogenetic distance (Figure 1A). The mammalian Latrophilin 1 homolog was identified through its capacity to bind the black widow spider venom component α -latrotoxin (α -LTX; Davletov et al., 1996; Krasnoperov et al., 1996), which induces a surge of vesicular release from synaptic terminals and neuroendocrine cells through formation of membrane pores (Orlova et al., 2000; Rosenthal and Meldolesi, 1989). Latrophilin 1/ADGRL1 was suggested to partake in presynaptic calcium homeostasis by interacting with a teneurin ligand (Silva et al., 2011) and in *trans*-cellular adhesion through interaction with neurexins 1 β and 2 β (Boucard et al., 2012). Further, engagement of Latrophilin 3/ADGRL3 with FLRT proteins may contribute to synapse development (O'Sullivan et al., 2014). The role of Latrophilins in the nervous system thus appears complex.

Here we have used a genomic engineering approach to remove and modify the Latrophilin locus *dCirl*, the only Latrophilin homolog of *Drosophila melanogaster*. We report that *dCirl* is required in chordotonal neurons for adequate sensitivity to gentle touch, sound, and proprioceptive feedback during larval locomotion. This indicates an unexpected role of the aGPCR Latrophilin in the recognition of mechanosensory stimuli and provides a unique in vivo demonstration of a GPCR in mechanosensation.

RESULTS

Genomic Engineering of a *dCirl* Null Allele

Drosophila melanogaster possesses a single Latrophilin homolog *dCirl/CG8639* (Figure 1C). We pursued a genomic engineering strategy to generate an incontestable *dCirl* null allele by homologous recombination. We replaced a fragment containing the complete *dCirl* open reading frame (ORF), part of the 5' intergenic region encoding the putative *dCirl* promoter, and the 5' and 3' UTRs with an *attP* site for subsequent phiC31-mediated

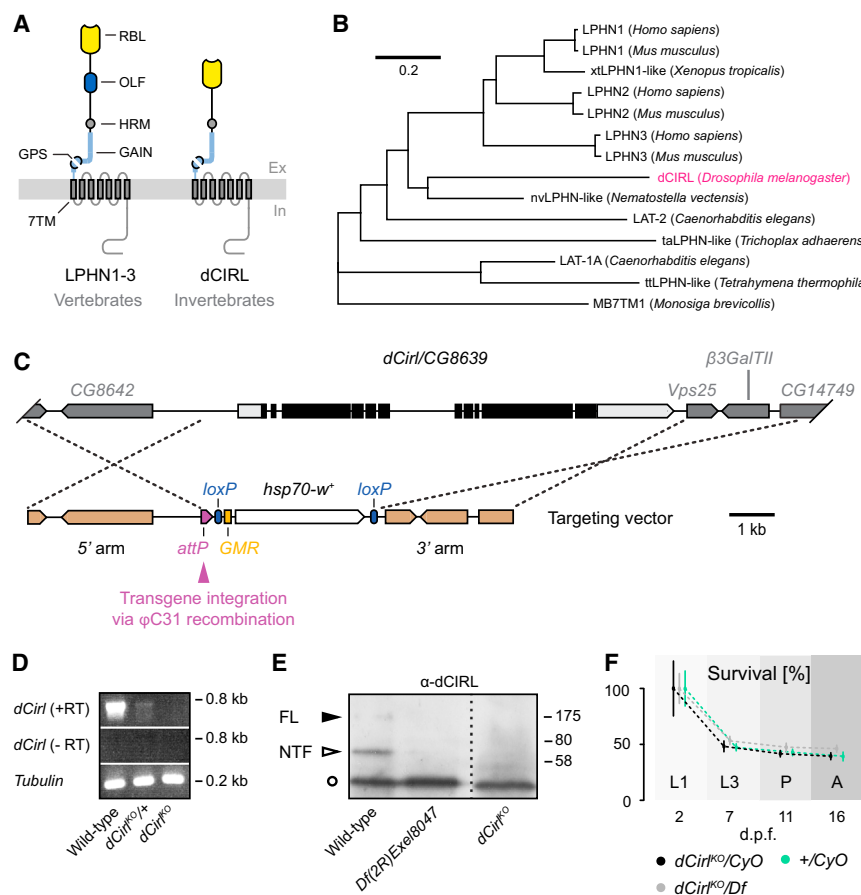


Figure 1. Construction of a *dCirr*^{KO} Allele and a Modifiable *dCirr* Locus

(A) Conserved domain structure of the Latrophilin subfamily of aGPCR containing RBL, OLF (present only in vertebrates), HRM, GAIN, and 7TM domains (N → C order).

(B) Phylogenetic analysis of dCIRL shows ancient conservation of Latrophilins from ciliates to humans.

(C) Genomic organization and targeting strategy of the *dCirr/CG8639* locus. See also Figures S1A–S1C.

(D and E) Confirmation of the *dCirr*^{KO} allele. (D) RT-PCR shows loss of *dCirr* transcripts in the *dCirr*^{KO} strain. (E) Anti-dCIRL antiserum detects no signal in protein extracts from *dCirr*^{KO} and *Df(2R)Exel8047* flies. In extracts of WT flies, two specific bands are detected that correspond to full-length (~180 kDa; closed arrowhead) and autoproteolyzed dCIRL (~70 kDa; open arrowhead). An unspecific signal (open circle) detected by the antiserum served as loading control. FL, full-length; NTF, N-terminal fragment. See also Figures S1D and S1E.

(F) Lethality phase analysis of *dCirr*^{KO} animals. Survival rates of *dCirr*^{KO} animals are indistinguishable from genetic controls throughout larval (L1, L3), pupal (P), and adult (A) stages. d.p.f., days post-fertilization. Data are represented as mean ± SEM.

transgene insertion, and a floxable *hsp70-white* selection cassette (Figures 1C and S1). A recombinant strain, termed *dCirr*^{KO}, was selected and backcrossed into *w*¹¹¹⁸ background for 15 generations before further analyses.

First, we established that *dCirr*^{KO} is a null allele by transcribing cDNA libraries from *dCirr*^{KO} and control flies, which showed no residual transcript in *dCirr*^{KO} homozygotes (Figure 1D). We prepared protein extracts from WT larvae and larvae homozygous for *dCirr*^{KO} or *Df(2R)Exel8047*, a small deficiency uncovering the *dCirr* locus. Immunodetection with a polyclonal antiserum raised against a peptide in the extracellular domain (ECD) of dCIRL showed two bands corresponding to the full-length (approximately 185 kDa) and autoproteolyzed receptor (N-terminal fragment [NTF], approximately 77 kDa; C-terminal fragment [CTF], approximately 108 kDa) cleaved at the GPS motif in WT extracts. Both bands were absent from samples prepared from *dCirr*^{KO} and *Df(2R)Exel8047* homozygotes (Figure 1E). We conclude that *dCirr*^{KO} is a protein null allele.

dCirr Is Required for Coordinated Locomotion

To investigate whether *dCirr* exerts developmental functions, we conducted a lethal phase analysis. Intriguingly, *dCirr*^{KO}/*Df(2R)Exel8047* transheterozygotes developed indistinguishably from controls throughout embryonic, larval, and adult phases, indicating that *dCirr* is not essential for overt development and viability in *Drosophila* (Figure 1F).

During this investigation, we noted that *dCirr*^{KO} larvae exhibit a conspicuous crawling pattern and travel less distance than controls (Movie S1). While in control larvae the forward motion phase occupies the majority of the motility cycle, *dCirr*^{KO} animals spent extended amounts of time in head swing episodes, which resulted in increased pausing of larvae and decreased net crawling distances (Figures 2A and 2B; Table S1; Movie S1). This defect was rescued to the WT level by reinsertion of a genomic fragment at the *attP* site in the *dCirr*^{KO} strain generating *dCirr*^{rescue} larvae (Figure 2B; Table S1; Movie S1).

These results imply an unexpected role of *dCirr* in shaping locomotion. In addition, they validated our genomic engineering approach to remove *dCirr* function and to generate allelic variants of the *dCirr* locus.

dCIRL Is Expressed in Chordotonal Neurons

Larval crawling is a complex behavior controlled through motor and central pattern generator neurons of the CNS (Jan and Jan, 1976; Suster and Bate, 2002) and adjusted by sensory feedback from afferent neurons of the peripheral nervous system (Caldwell et al., 2003; Cheng et al., 2010).

To determine in which cells *dCirr* is expressed, we conceived a *dCirr* transcriptional reporter allele (*dCirr*^{GAL4}) that contained an optimized *gal4.2::p65* cassette at the start codon of the genomic *dCirr* ORF (Figure 2C). Among other neuron types (Figure 2D; data not shown), *dCirr*^{GAL4} > *UAS-mCD8::GFP* expression was most prominent in larval pentascolopodial chordotonal organs (lch5; Figures 2D and 2E). Chordotonal organs (cho) are compound

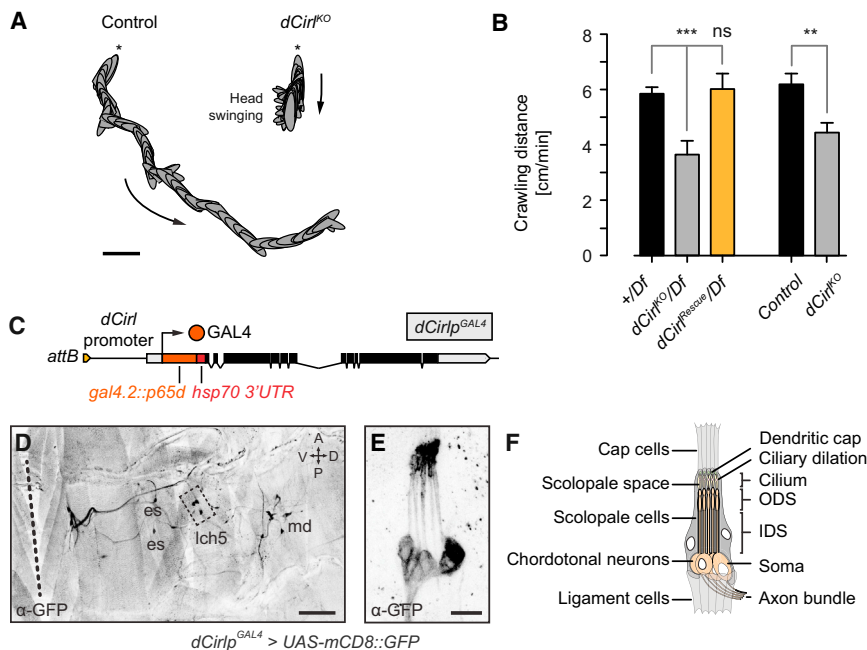


Figure 2. *dCirl* Is Required for Larval Locomotion and Expressed in *lch5* Chordotonal Neurons

(A) Loss of *dCirl* results in increased pausing and excessive head swing behavior. Reconstructions of 60 frames for each genotype representing 36 s of recording. Arrows indicate direction of crawling motion, and asterisks mark the start frames. Scale bar represents 5 mm. See also [Movie S1](#).

(B) Quantification of crawling distance. Data are represented as mean \pm SEM. See also [Table S1](#) and [Movie S1](#).

(C) Transgene structure of transcriptional reporter (*dCirl^{GAL4}*).

(D) *dCirl^{GAL4}* expresses in several peripheral sensory neuron types including type I and type II neurons. Dashed line indicates midline. es, external campaniform sensilla; *lch5*, pentascolopodial organ; md, multidendritic neurons. Scale bar represents 100 μ m. The dashed rectangle is magnified in (E).

(E) Strong *dCirl^{GAL4}* expression observed in *lch5* lateral chordotonal organs. Scale bar represents 20 μ m.

(F) Anatomy of a third instar larval pentascolopodial organ. IDS, inner dendritic segment; ODS, outer dendritic segment.

sensory structures that govern the perception of a wide range of mechanical inputs in *Drosophila*, including proprioceptive stimuli, gentle touch, and sound/vibration (Figure 2F; Kernan, 2007).

dCirl Is Required for the Function of Chordotonal Organs

To elucidate whether *dCirl* contributes to chordotonal function, we obtained an established score of the responsiveness of larvae toward gentle touch. In this assay, homozygous and heterozygous control larvae exhibited tactile sensitivities comparable to previously published control genotypes (Caldwell et al., 2003; Kernan et al., 1994; Yan et al., 2013). We found that *dCirl^{KO}* animals indeed exhibited diminished touch sensitivity (Figure 3A; Table S2). This was specifically due to loss of *dCirl*, as the phenotype in *dCirl^{KO}/Df(2R)Exel8047* transheterozygotes remained indistinguishable from *dCirl^{KO}* homozygotes, whereas *+Df(2R)Exel8047* animals exhibited normal touch sensitivity. Further, in *dCirl^{Rescue}* larvae, touch sensitivity was rescued to control level (Figure 3A; Table S2).

To exclude that *dCirl*'s impact on locomotion was conferred via other neurons, we performed a cell-specific rescuing assay with a *20xUAS-dCirl* genomic rescuing transgene, in which the *dCirl* promoter region was replaced with an optimized *20xUAS-IVS* promoter cassette (Figure 3B). We selected *GAL4* drivers with expression domains in motor neurons (*ok6-GAL4*), in all type II sensory neurons (*21-7-GAL4*), and only in chordotonal neurons (type I sensory neurons; *iav-GAL4*). With this set of *GAL4* lines, we drove expression of the *20xUAS-dCirl* rescuing transgene in the *dCirl^{KO}* background and scored for touch sensitivity. Intriguingly, the sensory deficit was rescued only upon *dCirl* re-expression in chordotonal neurons (Figures 3C and S2A; Table S2). Similarly, chordotonal neuron-specific expression of *dCirl* restored normal crawling of *dCirl^{KO}* larvae (Figures 3D and S2B; Table S1).

The Structure of Chordotonal Neurons Appears Unaffected in *dCirl^{KO}* Mutants

Chordotonal organs and their monociliated type I sensory neurons possess an intricate structure that is relevant for their mechanosensory properties (Figure 2F; Eberl and Boekhoff-Falk, 2007). Consequently, we performed immunostainings to assess the subcellular location of the established chordotonal marker proteins NOMPC (*no mechanoreceptor potential C*) and EYS/SPAM (*eyes shut/spacemaker*) in chordotonal cilia of *dCirl^{KO}* larvae and found no differences in extent, location, or structure of these markers (Figures 3E–3H, S2C, and S2D).

Also, *iav-GAL4* positive chordotonal neuron somata, dendrites, and axonal projections revealed no morphological abnormalities (Figures S2E and S2F; Table S3). Altogether, these results demonstrate that *dCirl* is dispensable for the development and morphology of chordotonal sensory neurons.

dCirl Modulates the Absolute Electrical Activity of Chordotonal Neurons in Response to Mechanical Stimuli

To directly interrogate the function of chordotonal neurons, vibration stimuli were delivered to the cap cells of *lch5* using a piezoelectrically actuated glass probe (Figure 4A). The probe tip was placed at the cap cells of the *lch5*, which are mechanically linked to the apical portions of chordotonal neurons and scolopale cells through an extracellular matrix (dendritic cap; Chung et al., 2001) and septate junctions (Carlson et al., 1997), respectively (Figures 2F and 4A). While applying frequencies from 100–1,500 Hz (Figure S3A), we simultaneously recorded action currents from the axon bundle directly after its exit from the challenged *lch5* (Figure 4A).

Without mechanical stimulation, *dCirl^{KO}* *lch5* were spontaneously active, albeit at a slightly lower frequency than in WT

animals (Table S4A). Vibration triggered an increase in action current frequencies of WT *Ich5*, consistent with previous work (Figures 4B and 4C; Table S4A; Zhang et al., 2013). In our preparation, peak activity of neuronal responses was reached at stimulation frequencies around 900 Hz (Figures 4B and 4C; Table S4A). Most intriguingly, *dCirl*^{KO} larvae displayed significantly lower absolute action current frequencies across the entire stimulation spectrum (Figures 4B and 4C), which was fully compensated through the *dCirl*^{Rescue} allele (Figure S3B; Table S4B).

***dCirl* Modulates the Relative Mechanosensory Response of Chordotonal Neurons**

Sensory perception and encoding rely on the ability to contrast evoked from spontaneous activity in the principal sensory neuron. We thus quantified the proportional chordotonal response toward mechanostimulation, i.e., the ratio between evoked and spontaneous spiking activity (R_d ; Figure S3A), as a measure of the chordotonal neurons' facility to distinguish signal from noise. The discrimination ratio R_d in control *Ich5* neurons peaked around 900 Hz, suggesting that signal perception and/or encoding is most effective in this range of mechanostimulation. In contrast, *dCirl*^{KO} chordotonal neurons showed largely reduced R_d values over several vibration frequencies (Figure S3D; Table S4C). To detail the response profile across the entire stimulation spectrum, we statistically compared the R_d values for any pair of stimulation frequencies and derived discrimination matrices illustrating blurred mechanosignal discrimination in the absence of *dCirl* (Figures 4D, 4E, S3E, and S3F). This demonstrates that, besides modulating the absolute spiking activity of chordotonal neurons, *dCirl* is also necessary for their relative response toward mechanical stimuli.

Intriguingly, when *dCirl* was re-expressed in mutant chordotonal neurons through the *iav-GAL4* driver, the phenotype was partially rescued: the relative mechanosensory responses were re-established (Figures S3D and S3G), while absolute firing frequencies were not recovered (Figure S3C). This implies that *dCirl* cell autonomously modulates the relative response to mechanical stimulation, likely through the metabotropic activity of its CTF. In addition, *dCirl* may be required in other cells, e.g., for an intercellular homodimeric interaction (Prömel et al., 2012), to regulate absolute spiking frequency. Alternatively, as production of the receptor through the GAL4/UAS system is unlikely to restore endogenous expression levels, this may preclude the generation of a physiological evoked response frequency from the neurons.

***dCirl* Is Required for the Larval Startle Response to Sound Stimuli**

To corroborate the impact of *dCirl* on *Ich5* function with an independent assay, we examined the startle-freeze reaction of larvae toward a pure sine wave tone of 900 Hz (Zhang et al., 2013). We observed that *dCirl*^{KO} larvae exhibited diminished startle response scores at all sound pressure levels (SPLs) tested (Figures 4F and 4G; Table S5). This defect was rescued in *dCirl*^{Rescue} animals (Figure 4F; Table S5). Remarkably, at lower (60 dB) and higher (90 dB) sound pressure level (SPL), the responses of *dCirl*

and control neurons converged (Figures 4F and 4G; Table S5). This indicates that principal sound detection, i.e., the mechanotransduction complex, functions without *dCirl* but that its activation threshold appears increased in *dCirl*^{KO} larvae and is SPL dependent.

Taken together, *dCirl*^{KO} larval responses toward vibrational and acoustical stimulation place the function of *dCirl* at the level of mechanotransduction or spike initiation of chordotonal neurons and upstream of synaptic transmission.

***dCirl* Genetically Interacts with Components of the Molecular Mechanotransduction Apparatus**

In order to test this model, we evaluated genetic interactions of *dCirl* with the mechanotransduction machinery. We constructed double mutants of *dCirl*^{KO} in combination with hypomorphic alleles of the TRP channel subunits TRPN1/NOMPC (*nompC*^{f00642}; Sun et al., 2009) and TRPV/Nanchung (*nan*^{36a}; Kim et al., 2003), which forms a heteromeric complex with the subunit IAV (Inactive) in the proximal cilium of chordotonal neurons (Gong et al., 2004). In an epistasis assay, we tested crawling distances of singly and doubly mutant larvae.

Similar to *dCirl*^{KO}, also *nompC*^{f00642} and *nan*^{36a} mutants displayed locomotion activity but traveled less than control animals (control > *nompC*^{f00642} > *dCirl*^{KO} > *nan*^{36a}; Figure 5A; Table S1). This allowed us to study the genetic interaction of *dCirl* with either *trp* channel subunit. Interestingly, we did not observe simple additivity of crawling distance deficits in *dCirl*^{KO}, *nompC*^{f00642} and *dCirl*^{KO}; *nan*^{36a} double mutants (Figure 5A; Table S1). Instead, *dCirl*^{KO} animals behaved epistatically to *nompC*^{f00642} and *nan*^{36a}, implying that *dCirl* acts upstream of the *trp* subunits. Consistent with this model, overexpressing a *nompC::GFP* fusion transgene under *iav-GAL4* control in *dCirl*^{KO} larvae partially rescued the *dCirl*^{KO} crawling defect (Figure 5A). Intriguingly, our analysis also showed that removing *dCirl* from *nompC*^{f00642} or *nan*^{36a} backgrounds results in inverse outcomes, i.e., decreased and increased crawling distances, respectively (Figure 5A). This suggests that *dCirl* enhances *nompC* activity while curtailing *nan* function. These experiments demonstrate that *dCirl* genetically interacts with essential elements of the mechanotransduction machinery in chordotonal cilia.

The *dCirl* Promoter Contains *cis*-Regulatory Elements Required for Specialization of Mechanosensory Cilia

Genes involved in the functionalization of chordotonal cilia into a mechanosensory structure are controlled through recognition sites for the transcriptional activators RFX and Fd3F (Figures S4A–S4D; Newton et al., 2012).

We analyzed the 2.2-kb intergenic region upstream of the *dCirl* translational start site for the presence of RFX and Fd3F binding sites (Emery et al., 1996; Laurençon et al., 2007). Indeed, in the 200-bp fragment upstream of the *dCirl* start codon, we identified a pair of RFX and Fd3F recognition sites (Figure 5B), which were also conserved in other *Drosophila* species (Figures S4E and S4F).

This promotes the notion that the aGPCR *dCirl* is part of a gene set, which functionalizes the cilium of chordotonal neurons into a mechanosensitive subcellular compartment.

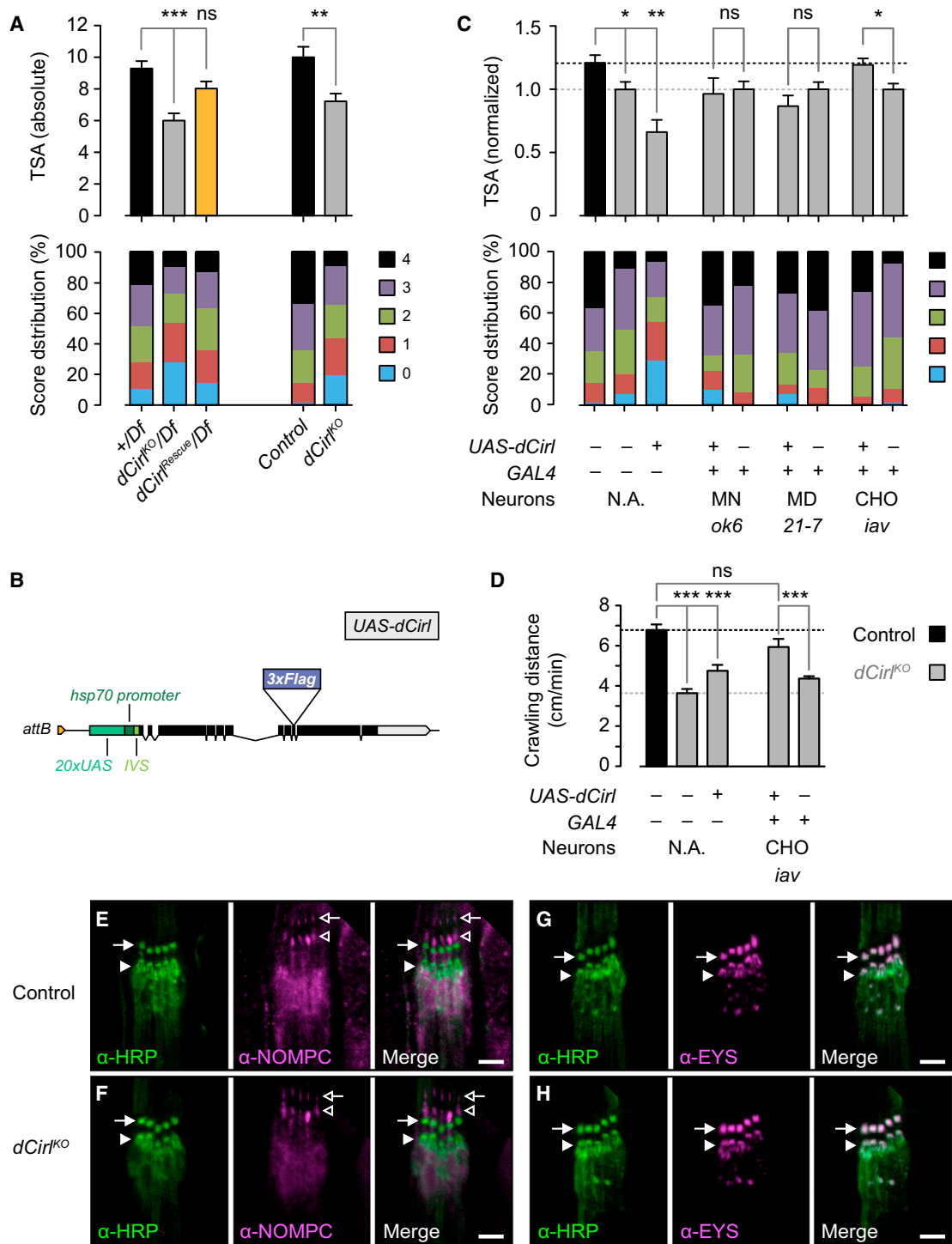


Figure 3. *dCirl* Is Required for Mechanosensation through Chordotonal Organs

(A) Loss of *dCirl* causes reduction in touch sensitivity. The upper shows the averaged results per genotype from 4-fold testing of individual larvae, and the lower contains the score distribution. 0, no response; 1, pause; 2, recoil; 3, retraction and deviation from stimulus $<90^\circ$; and 4, retraction and deviation from stimulus $>90^\circ$. See also Table S2.

(B) Structure of *UAS-dCirl* rescuing transgene.

(C) Cell-specific rescue reveals *dCirl* function is specifically required in chordotonal organs (CHO) for full-touch sensitivity, but not in multidendritic (type II; MD) or motor neurons (MNs). Dashed line in black indicates performance of WT, and dashed line in gray indicates performance of *dCirl*^{KO} animals. See also Figure S2 and Table S2.

(legend continued on next page)

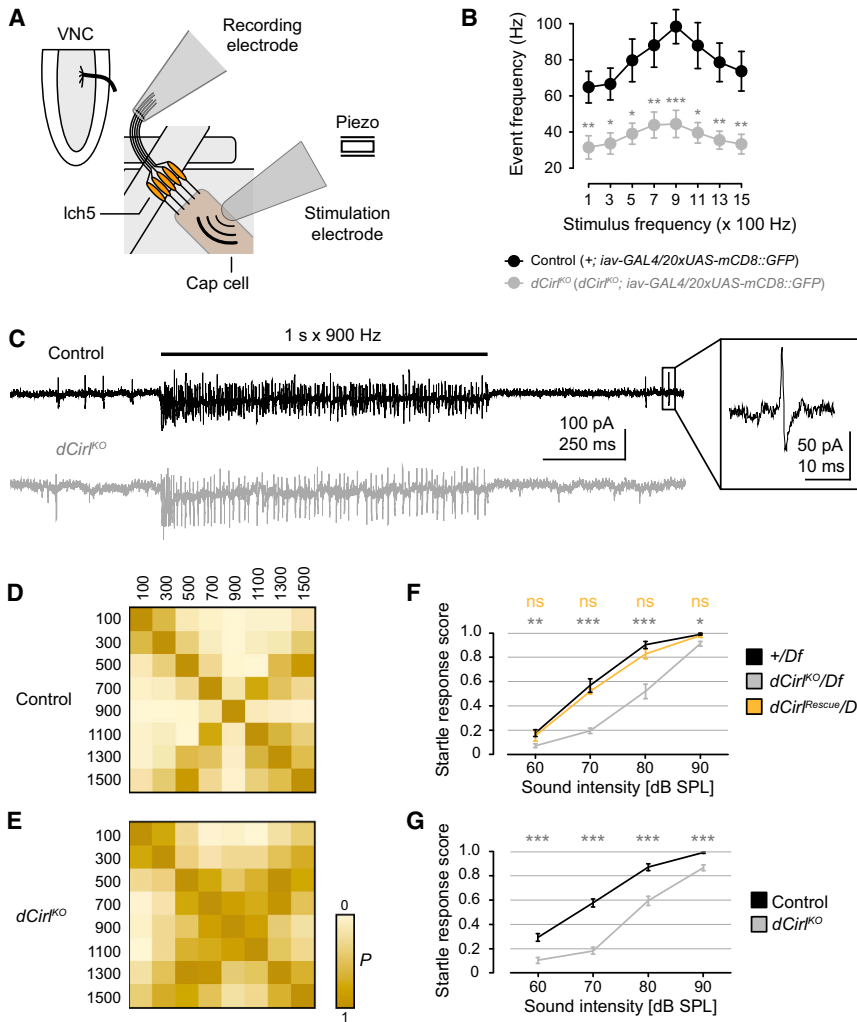


Figure 4. *dCirl* Is Necessary for the Physiological Response to Mechanical Stimulation in Larval Chordotonal Organs

(A) Preparation to probe ICh5 neuron responses to mechanical stimulation.

(B) Quantification of action current frequencies evoked by mechanical stimulation. See also Table S4.

(C) Representative recordings from ICh5 axons of control and *dCirl*^{KO} animals at 900-Hz stimulation. Boxed region shows a spontaneous event.

(D and E) Statistical comparisons of R_d values (color coded). Adjacent vibration stimuli elicit significantly different relative spiking responses in control ICh5 (D), whereas *dCirl* removal blurs mechanosignal discrimination. See also Figures S3E–S3G.

(F and G) Larval startle responses toward a 900-Hz sine sound of increasing intensity. Hemizygous (F) and homozygous (G) *dCirl*^{KO} animals show a reduced startle response (F); p values (versus +/Df) are indicated above each data point colored according to the genotype. See also Table S5.

Data in (B), (F), and (G) are represented as mean \pm SEM.

DISCUSSION

Latrophilin/*dCirl* Modulates Mechanosensation

In the current analysis, we provide multiple lines of evidence to support that Latrophilin/*dCirl*, one of only two aGPCRs in the fly, is a critical regulator of mechanosensation through chordotonal neurons in *Drosophila* larvae:

- (1) Larval chordotonal organs respond to tactile stimuli arising through gentle touch, mechanical deformation of the larval body wall and musculature during the locomotion cycle, and vibrational cues elicited through sound (Caldwell et al., 2003; Hughes and Thomas, 2007). We determined that registration of all these mechanical qualities is reduced in the absence of *dCirl* based on behavioral assays.

in chordotonal dendrites, the site of mechanotransduction and receptor potential generation, or somata, where action potentials are likely initiated (Kernan, 2007). Further, the ability of chordotonal neurons to generate mechanical responses relative to their background spike activity appears to be modulated by *dCirl*.

- (2) We established that behavioral defects can be rescued by re-expression of *dCirl* in chordotonal neurons, one of several cell types with endogenous *dCirl* expression.
- (3) Mechanically stimulated ICh5 neurons lacking *dCirl* responded with action currents at approximately half the control rate across a broad spectrum of stimulation frequencies, providing direct functional evidence for a role of *dCirl*
- (4) Combining *dCirl*^{KO} with strong hypomorphs of *trp* homologs, ion channels that are directly responsible for the conversion of mechanical stimulation into electrical signals within chordotonal neurons (Cheng et al., 2010; Gong et al., 2004; Kim et al., 2003; Yan et al., 2013; Zhang et al., 2013), implies that *dCirl* operates upstream of them.
- (5) The *dCirl* promoter contains a RFX/Fd3F transcription factor signature that implicates *dCirl* in the mechanosensitive specialization of sensory cilia (Newton et al., 2012).

(D) Re-expression of *dCirl* only in chordotonal organs rescues the crawling defect. Data in upper (A), (C), and (D) are represented as mean \pm SEM. See also Figure S2 and Table S1.

(E–H) Markers HRP, EYS/SPAM, and NOMPC in WT and *dCirl*^{KO} larval chordotonal neurons are indistinguishable. NOMPC/TRPN1 (E and F) is located in the distal cilium (open arrows), including the ciliary dilation (open arrowheads). HRP (E–H) and EYS/SPAM (G and H) form a collar around the cilium (closed arrows) beneath the ciliary dilation and mark the inner dendritic segment membrane (closed arrowheads). Scale bars represent 5 μ m. See also Figure S2 and Table S3.

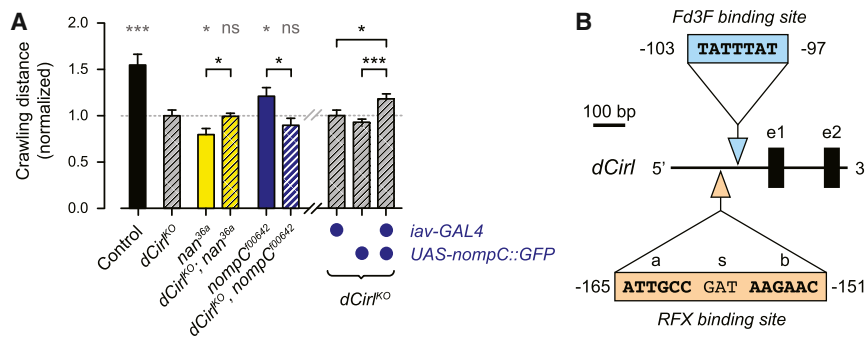


Figure 5. *dCirl* Genetically Interacts with the Mechanotransduction Machinery of Chordotonal Cilia

(A) Normalized score of larval crawling distance for epistasis testing between *dCirl* and *trp* homologs *nompC* and *nan*. Dashed line in gray indicates performance of *dCirl^{KO}* (left) and *dCirl^{KO}; iav-GAL4/+* animals (right). Data are represented as mean ± SEM. See also Table S1.

(B) Location and sequence of putative RFX-binding (orange arrowhead) and Fd3F (blue arrowhead) binding sites identified in the *dCirl* promoter region. Half-sites a and b of the X box motif recognized by RFX transcription factors (in bold) are separated through a three-nucleotide spacer (s). e1, exon 1; e2, exon 2. See also Figure S4.

On the basis of these results, we propose that *dCirl* partakes in the process of mechanotransduction or spike initiation and transmission to promote sensory encoding.

Adhesion GPCRs: A Class of Metabotropic Mechanosensors

The classical model of GPCR activation has become the archetypical example for cellular perception of external signals. It comprises soluble ligands that bind to the extracellular portions of a cognate receptor, whereby receptor conformation is stabilized in a state that stimulates metabotropic effectors. Thus, GPCRs are primarily regarded as chemosensors due to the nature of their activating agents. The concept that GPCRs may also be fit to detect and transduce physical modalities, i.e., mechanical stimulation, has received little support thus far.

aGPCRs display an exceptional property among the GPCR superfamily in that they recognize cellular or extracellular ligands (Hamann et al., 1996). To date, only one ligand has proved adequate to induce intracellular signaling (Paavola et al., 2014), whereas for the vast majority of ligand-aGPCR interactions this proof either failed or is lacking (Langenhan et al., 2013). This implies that sole ligand recognition is generally not sufficient to induce a metabotropic response of aGPCRs. Thus, in addition to ligand engagement, our results suggest that mechanical load is a co-requirement to trigger the activity of dCIRL, a prototypical aGPCR homolog.

Recent findings place aGPCRs in the context of mechanically governed cellular functions (Yang et al., 2013), but how mechanical perception through aGPCR activity impinges on cell responses has not yet been established. In addition, the molecular structure of aGPCR is marked by the presence of a GPCR autoproteolysis inducing (GAIN) domain (Araç et al., 2012), which plays a paramount role in signaling scenarios for aGPCRs (Prömel et al., 2013). This domain type is also present in PKD-1/Polycystin-1-like proteins, which are required to sense osmotic stress and fluid flow in different cell types and are thus considered bona fide mechanosensors (Retailleau and Duprat, 2014). In addition, studies on EGF-TM7-, BAI-, and GPR56-type aGPCRs further showed that proteolytic processing and loss of NTF may figure prominently in activation of the receptors' metabotropic signaling output (Okajima et al., 2010; Paavola et al., 2011; Yang et al., 2011) and that mechanical forces ex-

erted through receptor-ligand contact are required for receptor internalization (Karpus et al., 2013).

dCirl is not the only aGPCR associated with mechanosensation. *Celsr1* is required during planar cell polarity establishment of neurons of the inner ear sensory epithelium (Curtin et al., 2003). Similarly, the very large G-protein-coupled receptor 1 (VLGR1) exerts an ill-defined developmental role in cochlear inner and outer hair cells, where the receptor connects the ankle regions of neighboring stereocilia (McGee et al., 2006). In addition, VLGR1 forms fibrous links between ciliary and apical inner segment membranes in photoreceptors (Maerker et al., 2008). Both cell types are affected in a type of Usher syndrome, a congenital combination of deafness and progressive retinitis pigmentosa in humans, which is caused by loss of *VLGR1* function (Weston et al., 2004). Although present evidence derived from studies of constitutively inactive alleles suggests a requirement for *Celsr1* and *VLGR1* aGPCR for sensory neuron development, their putative physiological roles after completion of tissue differentiation have remained unclear and should be of great interest.

Outlook

In the current model on *dCirl* function, aGPCR activity, adjusted by mechanical challenge, modulates the molecular machinery gating mechanotransduction currents or the subsequent initiation of action potentials and ensures that mechanical signals are encoded distinctly from the background activity of the sensory organ. Thereby, *dCirl* shapes amplitude and kinetics of the sensory neuronal response. Linking adequate physiological receptor stimulation to downstream pathways and cell function is an essential next step to grasp the significance of aGPCR function and the consequences of their malfunction in human conditions. The versatility of the *dCirl* model now provides an unprecedented opportunity to study the mechanosensory properties of an exemplary aGPCR and to uncover features that might prove of general relevance for the function and regulation of the entire aGPCR class.

EXPERIMENTAL PROCEDURES

Immunohistochemistry and Imaging of Chordotonal Neurons

Wandering third instar larvae were dissected in ice-cold Ca^{2+} -free HL-3 (Stewart et al., 1994), fixed in 4.0% paraformaldehyde for 10 min, blocked for 30 min

in PBT (PBS with 0.1 % Triton X-100; SigmaAldrich) containing 5% normal goat serum, and immunostained according to established protocols (Schmid and Sigrist, 2008). Preparations were incubated with the primary antibody at 4°C overnight and washed and incubated with secondary antisera for 2 hr at room temperature. Each incubation step was followed by two short washes and 3 × 20 min washes in PBT (0.05 % Triton X-100). The blocking step was carried out over night at 4°C using 1% PBT (1% Triton X-100) containing 2% BSA and 5% normal goat serum (NGS). Primary antibodies were added to fresh blocking solution and incubated for 24 hr at 4°C. Next, samples were washed four times for 30 min with PBS containing 0.1 % Tween. Secondary antibodies were diluted in PBS (0.1% Tween, 2% BSA, 5% NGS) and used for incubation overnight at 4°C. Samples were washed four times for 30 min with PBS containing 0.1% Tween and stored in Vectashield over night before mounting.

In each experiment, different genotypes were stained under the same conditions. Antibody dilutions used in the study are detailed in the [Supplemental Experimental Procedures](#). Confocal image stacks were obtained with a line-scanning confocal LSM 5 system (Zeiss) equipped with a 1.25 numerical aperture 63× oil-immersion objective.

Chordotonal Neuron Recordings

Male third instar larval preparations were immersed in extracellular saline (Zhang et al., 2013), and the lch5 was exposed by gentle removal of overlying muscles. The axon bundle was cut with fine scissors and sucked into a recording electrode to measure action currents. Mechanical stimuli of increasing frequency were delivered using a piezo-coupled, fire-polished glass electrode placed at the lch5 cap cells.

In all electrophysiological recordings, genotypes were blinded. Further details of patch clamp and chordotonal neuron recordings are provided in the [Supplemental Experimental Procedures](#).

Behavioral Assays

Larval Crawling Paradigm

The locomotion paths for each genotype were video recorded for 0.5 to 2 min using a digital camera. Briefly, wandering third instar larvae were positioned in an agarose (1%)–filled petri dish. Subsequently, movies were used to track the crawling path of single larvae. Digital measurements of traveled distances were obtained using the wrMTrck plugin (J.S. Pedersen, <http://www.phage.dk/plugins/wrmtrck.html>) for ImageJ (NIH).

Touch Sensitivity Paradigm

External touch sensitivity was tested on single third-instar larvae raised at 25°C. During linear locomotion in a petri dish (5 cm in diameter), larvae were gently touched with the tip of a von Frey filament (0.3 mN) on their anterior thoracic segments (Kernan et al., 1994), and a scoring system by (Caldwell et al., 2003) was applied and is described in more detail in the [Supplemental Experimental Procedures](#). Genotypes were blinded before scoring.

Startle Response Paradigm

Larvae of different genotypes were challenged with a series of 10 tones of 900 Hz; their startle reaction was video recorded and a startle response score obtained according to Zhang et al. (2013). Videos were shuffled and genotype blinded before scoring. For details, see the [Supplemental Experimental Procedures](#).

Statistical Analysis

Two-tailed Mann-Whitney tests of data sets against a respective WT background control were performed using Prism 5 (GraphPad Software) or SigmaPlot (Systat Software). In the figures, asterisks denote the level of significance: * $p \leq 0.05$, ** $p \leq 0.01$, *** $p \leq 0.001$. Data are presented as mean \pm SEM.

SUPPLEMENTAL INFORMATION

Supplemental Information includes Supplemental Experimental Procedures, four figures, five tables, and one movie and can be found with this article online at <http://dx.doi.org/10.1016/j.celrep.2015.04.008>.

AUTHOR CONTRIBUTIONS

N.S. analyzed proprioception, hearing, lch5 morphology, and genetic interactions of *dCirl* mutants. J.G. assessed touch sensation and lch5 structure. C.G. and D.L. performed electrophysiological recordings. R.F. constructed the *dCirl* null allele. V.L. built devices for behavioral scoring. R.J.K. and T.L. conceived the project, designed experiments, analyzed data, and coordinated the study. T.L. wrote the manuscript with assistance from all co-authors.

ACKNOWLEDGMENTS

This work was supported by grants from the German Research Foundation (DFG) to R.J.K. and T.L. (KI 1460/1-1, LA 2861/1-1, SFB 1047/Project A5, FOR 2149/TP1 and TP3). Fly strains were obtained from the Bloomington Stock Center (NIH P40OD018537) and the Harvard Exelixis deficiency collection. The authors thank H. Holzinger, M. Oppmann, U. Strobel, and C. Wirth for technical assistance and the following colleagues for materials and discussions: E. Buchner, M. Göpfert, M. Köttgen, M. Heckmann, Y.N. Jan, T. Raabe, P. Senthilan, S.J. Sigrist, S. Stowers, T.C. Südhof, C. Wegener, S. Younger, and K. Zinsmaier.

Received: June 8, 2014

Revised: March 9, 2015

Accepted: April 1, 2015

Published: April 30, 2015

REFERENCES

- Araç, D., Boucard, A.A., Bolliger, M.F., Nguyen, J., Soltis, S.M., Südhof, T.C., and Brunger, A.T. (2012). A novel evolutionarily conserved domain of cell-adhesion GPCRs mediates autoproteolysis. *EMBO J.* *31*, 1364–1378.
- Boucard, A.A., Ko, J., and Südhof, T.C. (2012). High affinity neuroligin binding to cell adhesion G-protein-coupled receptor C1RL1/latrophilin-1 produces an intercellular adhesion complex. *J. Biol. Chem.* *287*, 9399–9413.
- Caldwell, J.C., Miller, M.M., Wing, S., Soll, D.R., and Eberl, D.F. (2003). Dynamic analysis of larval locomotion in *Drosophila* chordotonal organ mutants. *Proc. Natl. Acad. Sci. USA* *100*, 16053–16058.
- Carlson, S.D., Hilgers, S.L., and Juang, J.L. (1997). Ultrastructure and blood-nerve barrier of chordotonal organs in the *Drosophila* embryo. *J. Neurocytol.* *26*, 377–388.
- Chachivili, M., Zhang, Y.-L., and Frangos, J.A. (2006). G protein-coupled receptors sense fluid shear stress in endothelial cells. *Proc. Natl. Acad. Sci. USA* *103*, 15463–15468.
- Cheng, L.E., Song, W., Looger, L.L., Jan, L.Y., and Jan, Y.N. (2010). The role of the TRP channel NompC in *Drosophila* larval and adult locomotion. *Neuron* *67*, 373–380.
- Chung, Y.D., Zhu, J., Han, Y., and Kernan, M.J. (2001). *nompA* encodes a PNS-specific, ZP domain protein required to connect mechanosensory dendrites to sensory structures. *Neuron* *29*, 415–428.
- Curtin, J.A., Quint, E., Tsipouri, V., Arkell, R.M., Cattanach, B., Copp, A.J., Henderson, D.J., Spurr, N., Stanier, P., Fisher, E.M., et al. (2003). Mutation of *Celsr1* disrupts planar polarity of inner ear hair cells and causes severe neural tube defects in the mouse. *Curr. Biol.* *13*, 1129–1133.
- Davletov, B.A., Shamotienko, O.G., Lelianova, V.G., Grishin, E.V., and Ushkarov, Y.A. (1996). Isolation and biochemical characterization of a Ca^{2+} -independent alpha-latrotoxin-binding protein. *J. Biol. Chem.* *271*, 23239–23245.
- Eberl, D.F., and Boekhoff-Falk, G. (2007). Development of Johnston's organ in *Drosophila*. *Int. J. Dev. Biol.* *51*, 679–687.
- Emery, P., Strubin, M., Hofmann, K., Bucher, P., Mach, B., and Reith, W. (1996). A consensus motif in the RFX DNA binding domain and binding domain mutants with altered specificity. *Mol. Cell. Biol.* *16*, 4486–4494.
- Fredriksson, R., and Schiöth, H.B. (2005). The repertoire of G-protein-coupled receptors in fully sequenced genomes. *Mol. Pharmacol.* *67*, 1414–1425.

- Gong, Z., Son, W., Chung, Y.D., Kim, J., Shin, D.W., McClung, C.A., Lee, Y., Lee, H.W., Chang, D.-J., Kaang, B.-K., et al. (2004). Two interdependent TRPV channel subunits, inactive and Nanchung, mediate hearing in *Drosophila*. *J. Neurosci.* *24*, 9059–9066.
- Hamann, J., Vogel, B., van Schijndel, G.M., and van Lier, R.A. (1996). The seven-span transmembrane receptor CD97 has a cellular ligand (CD55, DAF). *J. Exp. Med.* *184*, 1185–1189.
- Hughes, C.L., and Thomas, J.B. (2007). A sensory feedback circuit coordinates muscle activity in *Drosophila*. *Mol. Cell. Neurosci.* *35*, 383–396.
- Jan, L.Y., and Jan, Y.N. (1976). Properties of the larval neuromuscular junction in *Drosophila melanogaster*. *J. Physiol.* *262*, 189–214.
- Karpus, O.N., Veninga, H., Hoek, R.M., Flierman, D., van Buul, J.D., Vandenaeker, C.C., van Bavel, E., Medof, M.E., van Lier, R.A.W., Reedquist, K.A., and Hamann, J. (2013). Shear stress-dependent downregulation of the adhesion-G protein-coupled receptor CD97 on circulating leukocytes upon contact with its ligand CD55. *J. Immunol.* *190*, 3740–3748.
- Kernan, M.J. (2007). Mechanotransduction and auditory transduction in *Drosophila*. *Pflugers Arch.* *454*, 703–720.
- Kernan, M., Cowan, D., and Zuker, C. (1994). Genetic dissection of mechanosensory transduction: mechanoreception-defective mutations of *Drosophila*. *Neuron* *12*, 1195–1206.
- Kim, J., Chung, Y.D., Park, D.-Y., Choi, S., Shin, D.W., Soh, H., Lee, H.W., Son, W., Yim, J., Park, C.-S., et al. (2003). A TRPV family ion channel required for hearing in *Drosophila*. *Nature* *424*, 81–84.
- Krasnoperov, V.G., Beavis, R., Chepurny, O.G., Little, A.R., Plotnikov, A.N., and Petrenko, A.G. (1996). The calcium-independent receptor of alpha-latrotoxin is not a neurexin. *Biochem. Biophys. Res. Commun.* *227*, 868–875.
- Langenhan, T., Prömel, S., Mestek, L., Esmaeili, B., Waller-Evans, H., Hennig, C., Kohara, Y., Avery, L., Vakonakis, I., Schnabel, R., and Russ, A.P. (2009). Latrophilin signaling links anterior-posterior tissue polarity and oriented cell divisions in the *C. elegans* embryo. *Dev. Cell* *17*, 494–504.
- Langenhan, T., Aust, G., and Hamann, J. (2013). Sticky signaling—adhesion class G protein-coupled receptors take the stage. *Sci. Signal.* *6*, re3.
- Laurençon, A., Dubrulle, R., Efimenko, E., Grenier, G., Bissett, R., Cortier, E., Rolland, V., Swoboda, P., and Durand, B. (2007). Identification of novel regulatory factor X (RFX) target genes by comparative genomics in *Drosophila* species. *Genome Biol.* *8*, R195.
- Maerker, T., van Wijk, E., Overlack, N., Kersten, F.F.J., McGee, J., Goldmann, T., Sehn, E., Roepman, R., Walsh, E.J., Kremer, H., and Wolfrum, U. (2008). A novel Usher protein network at the periciliary reloading point between molecular transport machineries in vertebrate photoreceptor cells. *Hum. Mol. Genet.* *17*, 71–86.
- McGee, J., Goodyear, R.J., McMillan, D.R., Stauffer, E.A., Holt, J.R., Locke, K.G., Birch, D.G., Legan, P.K., White, P.C., Walsh, E.J., and Richardson, G.P. (2006). The very large G-protein-coupled receptor VLGR1: a component of the ankle link complex required for the normal development of auditory hair bundles. *J. Neurosci.* *26*, 6543–6553.
- Mederos y Schnitzler, M., Storch, U., Meibers, S., Nurwakagari, P., Breit, A., Essin, K., Gollasch, M., and Gudermann, T. (2008). Gq-coupled receptors as mechanosensors mediating myogenic vasoconstriction. *EMBO J.* *27*, 3092–3103.
- Newton, F.G., zur Lage, P.I., Karak, S., Moore, D.J., Göpfert, M.C., and Jarman, A.P. (2012). Forkhead transcription factor Fd3F cooperates with Rfx to regulate a gene expression program for mechanosensory cilia specialization. *Dev. Cell* *22*, 1221–1233.
- O’Sullivan, M.L., Martini, F., von Daake, S., Comoletti, D., and Ghosh, A. (2014). LPHN3, a presynaptic adhesion-GPCR implicated in ADHD, regulates the strength of neocortical layer 2/3 synaptic input to layer 5. *Neural Dev.* *9*, 7.
- Okajima, D., Kudo, G., and Yokota, H. (2010). Brain-specific angiogenesis inhibitor 2 (BAI2) may be activated by proteolytic processing. *J. Recept. Signal Transduct. Res.* *30*, 143–153.
- Orlova, E.V., Rahman, M.A., Gowen, B., Volynski, K.E., Ashton, A.C., Manser, C., van Heel, M., and Ushkaryov, Y.A. (2000). Structure of alpha-latrotoxin oligomers reveals that divalent cation-dependent tetramers form membrane pores. *Nat. Struct. Biol.* *7*, 48–53.
- Paavola, K.J., Stephenson, J.R., Ritter, S.L., Alter, S.P., and Hall, R.A. (2011). The N terminus of the adhesion G protein-coupled receptor GPR56 controls receptor signaling activity. *J. Biol. Chem.* *286*, 28914–28921.
- Paavola, K.J., Sidik, H., Zuchero, J.B., Eckart, M., and Talbot, W.S. (2014). Type IV collagen is an activating ligand for the adhesion G protein-coupled receptor GPR126. *Sci. Signal.* *7*, ra76.
- Pierce, K.L., Premont, R.T., and Lefkowitz, R.J. (2002). Seven-transmembrane receptors. *Nat. Rev. Mol. Cell Biol.* *3*, 639–650.
- Prömel, S., Frickenhaus, M., Hughes, S., Mestek, L., Staunton, D., Woollard, A., Vakonakis, I., Schöneberg, T., Schnabel, R., Russ, A.P., and Langenhan, T. (2012). The GPS motif is a molecular switch for bimodal activities of adhesion class G protein-coupled receptors. *Cell Rep.* *2*, 321–331.
- Prömel, S., Langenhan, T., and Araç, D. (2013). Matching structure with function: the GAIN domain of adhesion-GPCR and PKD1-like proteins. *Trends Pharmacol. Sci.* *34*, 470–478.
- Retailleau, K., and Duprat, F. (2014). Polycystins and partners: proposed role in mechanosensitivity. *J. Physiol.* *592*, 2453–2471.
- Rosenthal, L., and Meldolesi, J. (1989). Alpha-latrotoxin and related toxins. *Pharmacol. Ther.* *42*, 115–134.
- Schmid, A., and Sigrist, S.J. (2008). Analysis of neuromuscular junctions: histology and in vivo imaging. *Methods Mol. Biol.* *420*, 239–251.
- Silva, J.-P., Lelianova, V.G., Ermolyuk, Y.S., Vysokov, N., Hitchen, P.G., Berninghausen, O., Rahman, M.A., Zangrandi, A., Fidalgo, S., Tonevitsky, A.G., et al. (2011). Latrophilin 1 and its endogenous ligand Lasso/teneurin-2 form a high-affinity transsynaptic receptor pair with signaling capabilities. *Proc. Natl. Acad. Sci. USA* *108*, 12113–12118.
- Stewart, B.A., Atwood, H.L., Renger, J.J., Wang, J., and Wu, C.F. (1994). Improved stability of *Drosophila* larval neuromuscular preparations in haemolymph-like physiological solutions. *J. Comp. Physiol. A Neuroethol. Sens. Neural Behav. Physiol.* *175*, 179–191.
- Sun, Y., Liu, L., Ben-Shahar, Y., Jacobs, J.S., Eberl, D.F., and Welsh, M.J. (2009). TRPA channels distinguish gravity sensing from hearing in Johnston’s organ. *Proc. Natl. Acad. Sci. USA* *106*, 13606–13611.
- Suster, M.L., and Bate, M. (2002). Embryonic assembly of a central pattern generator without sensory input. *Nature* *416*, 174–178.
- Weston, M.D., Luijendijk, M.W.J., Humphrey, K.D., Möller, C., and Kimberling, W.J. (2004). Mutations in the VLGR1 gene implicate G-protein signaling in the pathogenesis of Usher syndrome type II. *Am. J. Hum. Genet.* *74*, 357–366.
- Yan, Z., Zhang, W., He, Y., Gorczyca, D., Xiang, Y., Cheng, L.E., Meltzer, S., Jan, L.Y., and Jan, Y.-N. (2013). *Drosophila* NOMPC is a mechanotransduction channel subunit for gentle-touch sensation. *Nature* *493*, 221–225.
- Yang, L., Chen, G., Mohanty, S., Scott, G., Fazal, F., Rahman, A., Begum, S., Hynes, R.O., and Xu, L. (2011). GPR56 Regulates VEGF production and angiogenesis during melanoma progression. *Cancer Res.* *71*, 5558–5568.
- Yang, M.Y., Hilton, M.B., Seaman, S., Haines, D.C., Nagashima, K., Burks, C.M., Tessarollo, L., Ivanova, P.T., Brown, H.A., Umstead, T.M., et al. (2013). Essential regulation of lung surfactant homeostasis by the orphan G protein-coupled receptor GPR116. *Cell Rep.* *3*, 1457–1464.
- Zhang, W., Yan, Z., Jan, L.Y., and Jan, Y.-N. (2013). Sound response mediated by the TRP channels NOMPC, NANCHUNG, and INACTIVE in chordotonal organs of *Drosophila* larvae. *Proc. Natl. Acad. Sci. USA* *110*, 13612–13617.
- Zou, Y., Akazawa, H., Qin, Y., Sano, M., Takano, H., Minamino, T., Makita, N., Iwanaga, K., Zhu, W., Kudoh, S., et al. (2004). Mechanical stress activates angiotensin II type 1 receptor without the involvement of angiotensin II. *Nat. Cell Biol.* *6*, 499–506.

Cell Reports

Supplemental Information

The Adhesion GPCR Latrophilin/CIRL

Shapes Mechanosensation

**Nicole Scholz, Jennifer Gehring, Chonglin Guan, Dmitrij Ljaschenko, Robin Fischer,
Vetrivel Lakshmanan, Robert J. Kittel, and Tobias Langenhan**

CONTENTS

- Supplemental Data

<i>Supplemental item</i>	<i>Relationship to main text and other supplemental items</i>
Figure S1	related to Figure 1
Figure S2	related to Figure 3
Figure S3	related to Figure 4
Figure S4	related to Figure 5
Table S1	related to Figures 2, 3, 5 and S2
Table S2	related to Figures 3 and S2
Table S3	related to Figure 3
Table S4	related to Figures 4 and S3
Table S5	related to Figure 4
Movie S1	related to Figure 2
- Supplemental Experimental Procedures
 - Fly culture conditions and stocks
 - Transgene construction
 - Ends-out targeting of *dCirl*
 - phiC31-mediated recombination into *dCirl^{KO}-attP*
 - Antibody production
 - Immunohistochemistry and imaging
 - Morphological assessment of L3 pentascolopodial organs
 - Immunoblots
 - RT-PCR
 - Lethal phase analysis
 - Electrophysiological analyses
 - Behavioral assays
 - Phylogenetic analysis
 - Determination of putative RFX and Fd3F binding sites in the *dCirl* promoter
- Supplemental References

SUPPLEMENTAL DATA

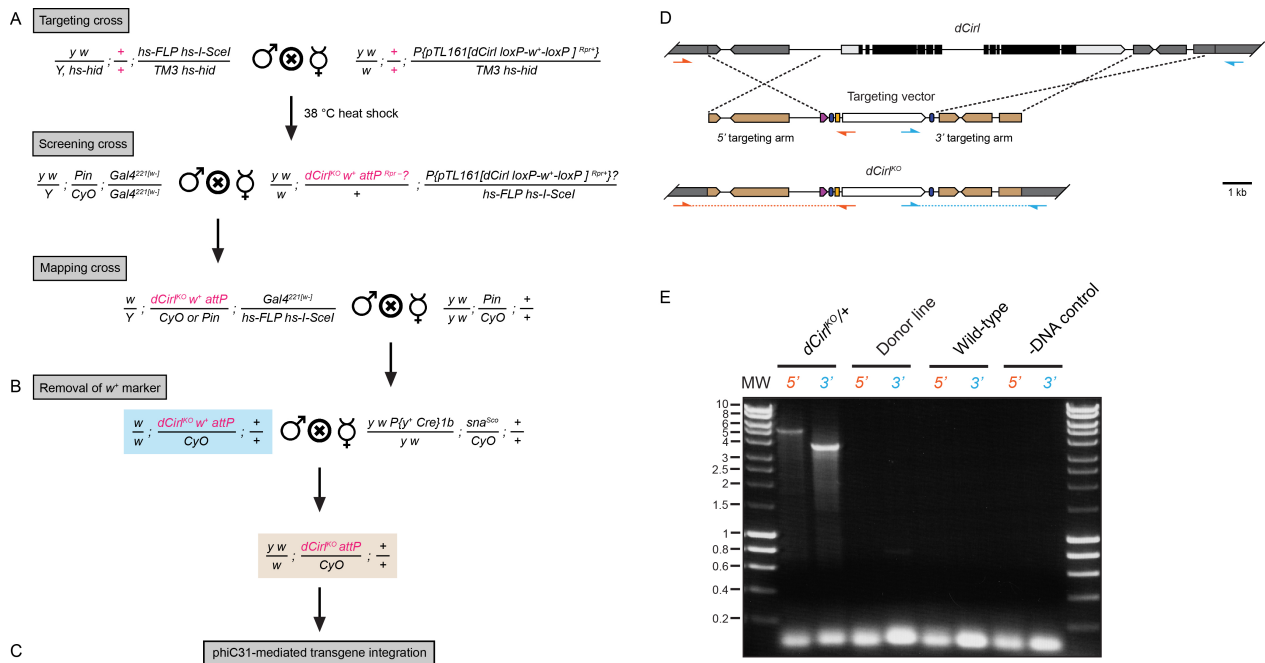


Figure S1. Genetic strategy for ends-out targeting of *dCirl* locus. Related to Figure 1.

(A) The *dCirl* locus was targeted and replacement was ensured through subsequent counter-selection of incorrectly or non-targeted recombinants, and mapping to the correct chromosomal location. Two recombinant fly strains were recovered from a screen of approx. 610,000 haploid genomes.

(B) In order to prepare the final *dCirl*^{KO} strain (blue shading) for re-integration of modified *dCirl* transgenes, the *w*⁺ marker was removed through Cre recombinase expression resulting in a *dCirl*^{KO} *w*⁻ fly strain (brown shading).

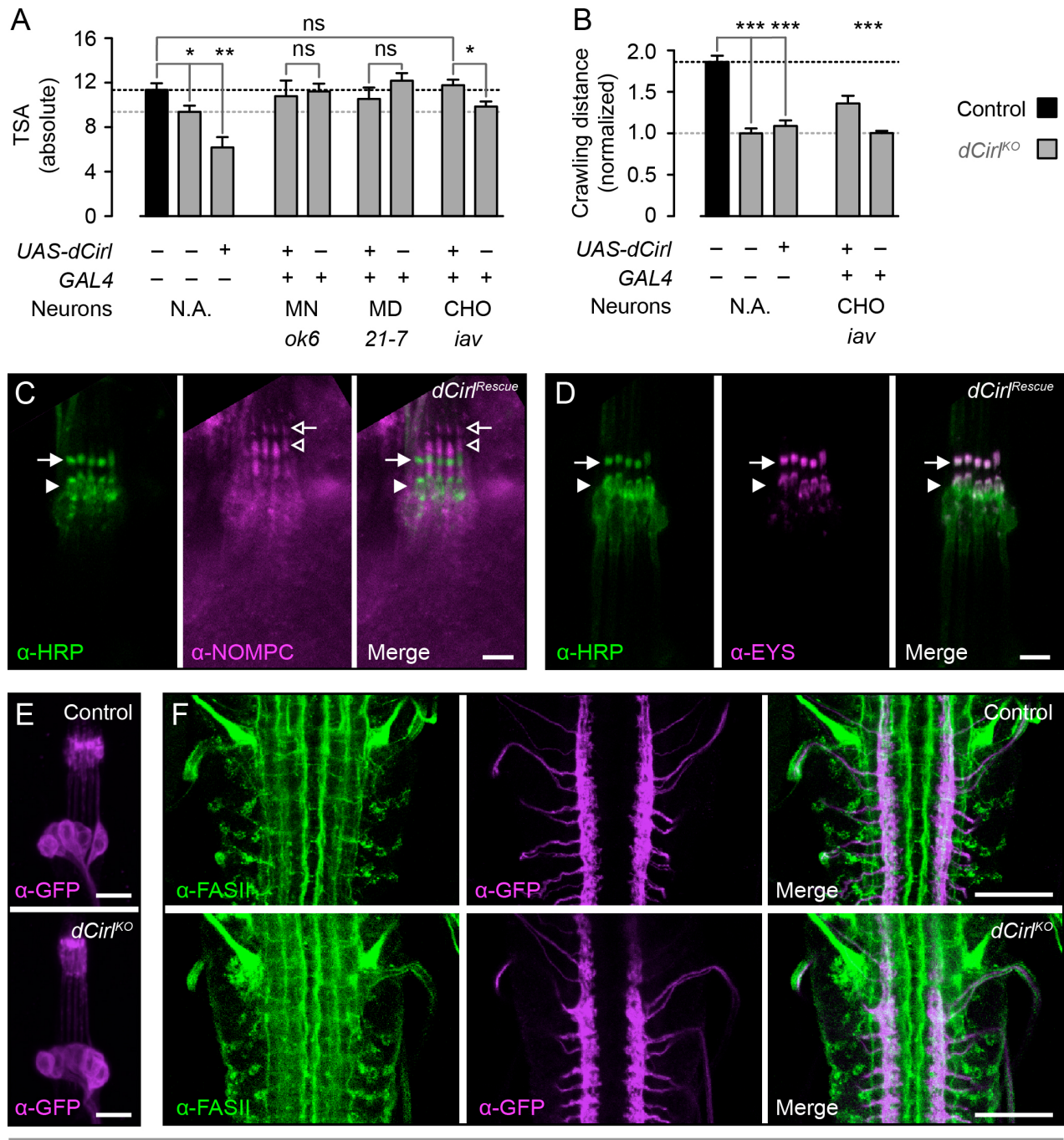
(C) This strain was used to integrate transgenes into the site of *dCirl* removal using the phiC31 method.

Target chromosomes and targeted events are marked in magenta throughout all genotypes listed. Figure adapted from (Huang et al., 2008).

(D) Targeting scheme of *dCirl* locus with positions of targeting arms (light brown), derived from genomic DNA, and the selection cassette. Positions of primers used to verify the targeting event at the *dCirl* locus are indicated (5' end of insertion: orange; 3' end of insertion: blue). Note that each primer pair consisted of one primer located outside the targeted, i.e. replaced, genomic DNA region, and one primer was positioned within the selection cassette encoded on the

targeting vector. Hence, only when the selection cassette replaced the genomic *dCirl* locus sequence, the primers were rendered in close position to each other so fragment amplification was feasible via long-range PCR.

(E) Long-range PCR results of the *dCirl*^{KO} strain used in the assays. Note that only genomic DNA from the engineered strain allows for amplification of 5' (5.3 kb) and 3' (3.8 kb) PCR fragments, but neither from the donor strain - the original transgenic line that carried the targeting vector used for *dCirl* targeting - nor from a wild-type control strain. The results indicate that indeed the *dCirl* locus was replaced through homologous recombination. MW = Molecular weight marker.



iav-GAL4 > 20xUAS-IVS-mCD8::GFP

Figure S2. Behavioral functions but not structure and protein composition of chordotonal organs depend on *dCirl*. Related to Figure 3.

(A) Absolute values for touch sensitivity assay (TSA) score after cell-specific rescue of *dCirl* function presented in Figure 3C. CHO, chordotonal organs; MD, multidendritic neurons; MN,

motor neurons. Dashed line in black indicates performance of wild-type, in grey of *dCirl*^{KO} animals.

(B) Normalized values for crawling distances after cell-specific rescue of *dCirl* function presented in Figure 3D.

(C and D) Localization of the markers HRP, NOMPC (C) and EYS/SPAM (D) in larval chordotonal neurons of *dCirl*^{Rescue} animals is indistinguishable from controls. Scale bars = 5 μ m.

(E) The overall structure of larval chordotonal neurons of the pentascolopodial organ is unaffected by loss of *dCirl*. Scale bars = 10 μ m. See also Table S3.

(F) Afferent axonal projections of chordotonal neurons into the neuropile of the VNC and the internal structure of the VNC as visualized by α -FASII counter-immunostaining are not affected in *dCirl*^{KO} larvae when compared with controls. Scale bars = 50 μ m.

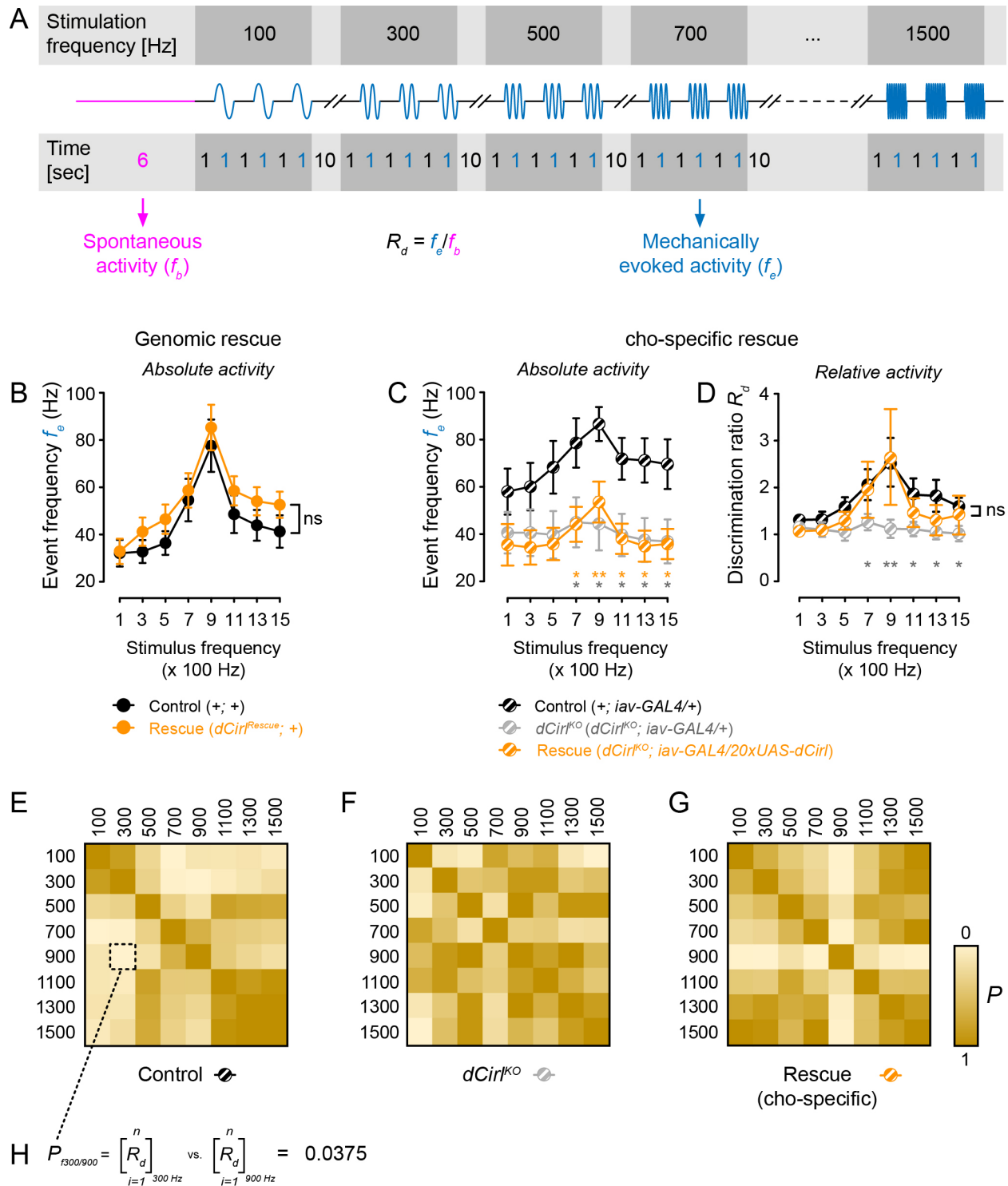


Figure S3. *dCirr* is required for the relative response of larval chordotonal neurons to mechanical stimulation. Related to Figure 4.

(A) Stimulation protocol to probe electrical responses of *lch5* upon mechanical stimulation.

(B) Action current frequencies evoked by mechanical stimulation are completely restored in *dCirl^{Rescue}* larvae.

(C and D) Restricted re-expression of *dCirl* in chordotonal neurons of *dCirl^{KO}* larvae does not rescue absolute action current frequency (C) but the relative spiking activity of lch5 (D) as evident from the discrimination ratio (R_d) plots.

(E-G) Discrimination matrices plotting pairwise comparison of R_d values obtained for each stimulation frequency couple show that loss of discriminatory power due to removal of *dCirl* (F) is partially rescued by chordotonal neuron-specific re-expression of *dCirl* (G).

(H) Exemplified calculation used to compare each R_d pair for discrimination matrix construction.

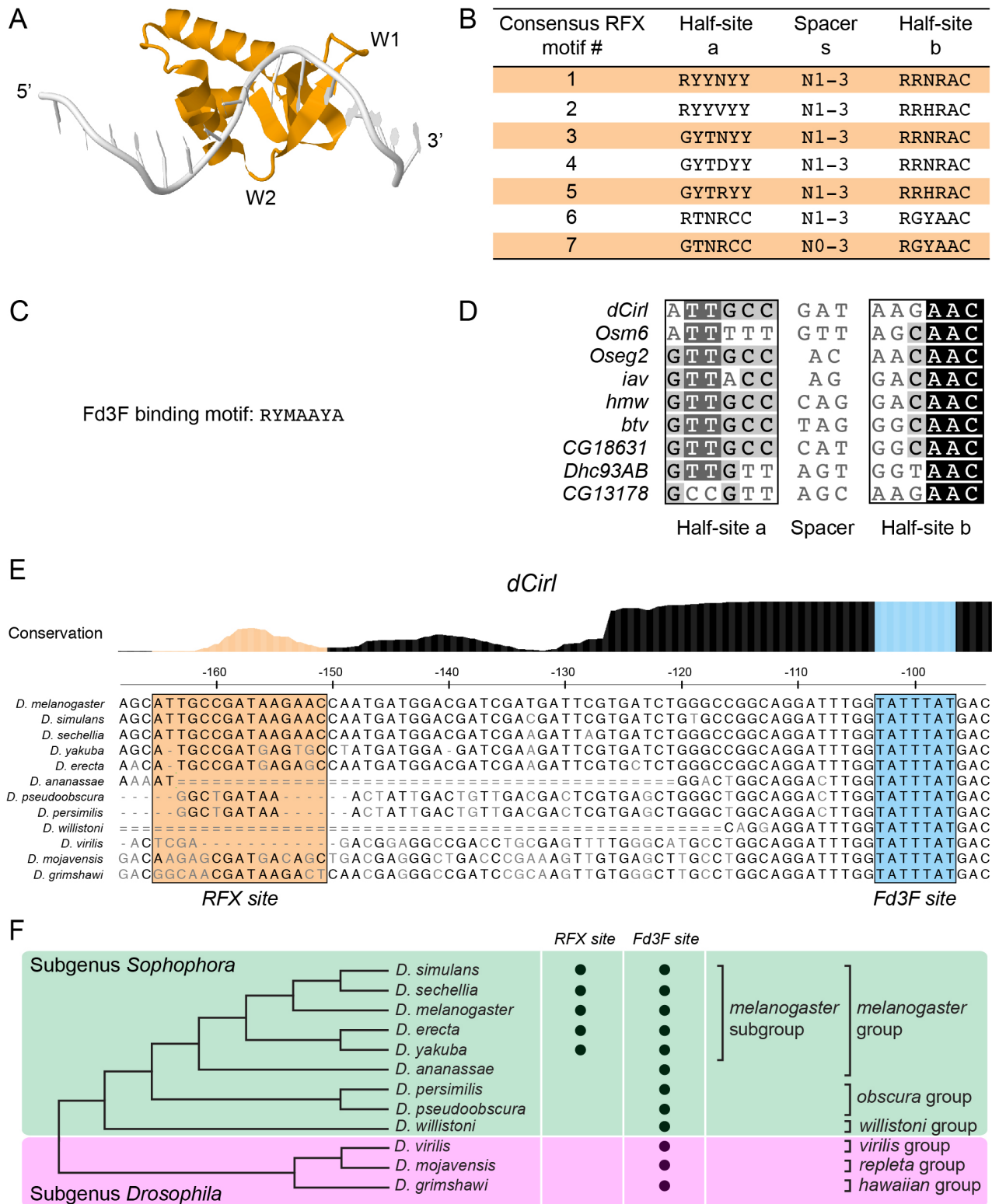


Figure S4. Identification of transcription factor binding sites involved in mechanosensory ciliary specialization in the *dCirl* promoter fragment. Related to Figure 5.

(A) Crystal structure of the human RFX1 (orange) bound to its target X-box motif (Gajiwala et al., 2000). W1 denotes wing 1, W2 wing 2 of the DNA-binding domain of hRFX1. Only one strand of the bound duplex oligonucleotide is shown.

(B) We examined the *dCirl* promoter region for the presence of consensus RFX binding sites, which resemble an imperfect palindromic X-box motif consisting of two half-sites recognized by the wings of the RFX DNA-binding domain. Nucleotide codes: D (A or G or T); H (A or C or T); M (A or C); N (any nucleotide); R (A or G); Y (C or T).

(C) Fd3F consensus motif used to screen the *dCirl* promoter (Benayoun et al., 2008). For nucleotide codes see (B).

(D) Alignment of the *dCirl* RFX-binding site (#1 in B) with similar sites present in promoter regions of genes expressed in ciliated sensory neurons of *Drosophila melanogaster*. These include genes responsible for mechanosensory transduction (*iav*, *nan*), motility (*Dhc93AB*, *btv*) and structural architecture (*rempA*, *Tektin-A*) of chordotonal cilia (Laurençon et al., 2007).

(E) The alignment of genome regions from 12 *Drosophila* species corresponding to a *dCirl* promoter fragment containing the identified RFX and Fd3F sites shows that the latter one is absolutely conserved, whereas the RFX binding site is only present in the *melanogaster* subgroup. Data exported from <http://genome.ucsc.edu>. Coordinates indicate relative position to the *dCirl* start codon in *D. melanogaster*.

(F) Summary of presence of RFX and Fd3F binding sites in *dCirl* homolog promoter regions from 12 *Drosophila* species. Phylogram adapted from (Drosophila 12 Genomes Consortium et al., 2007).

Table S1. Crawling distance measurements. Colors mark independent experimental data sets. Each top entry served as control. Values represent the mean \pm SEM. See also Movie S1. Related to Figures 2, 3, 5 and S2.

Genotype	Crawling distance [cm/min]	<i>n</i>	<i>P</i>	
Related to Figure 2B				
<i>w¹¹¹⁸; P{pTL161 w⁺}</i> ;	6.2 \pm 0.4	19	-	
<i>w¹¹¹⁸; dCirl^{KO} w⁺</i> ;;	4.5 \pm 0.4	18	.005	
<i>w[*]; +/Df(2R)Exel8047</i> ;;	5.9 \pm 0.3	11	-	
<i>w[*]; dCirl^{KO}/Df(2R)Exel8047</i> ;;	3.7 \pm 0.5	14	.001	
<i>w[*]; dCirl^{Rescue}/Df(2R)Exel8047</i> ;;	6.1 \pm 0.6	11	.718	
Related to Figures 3D and S2B				
<i>w^{1118...,,,}</i>	6.8 \pm 0.3	19	-	
<i>w¹¹¹⁸; dCirl^{KO} w⁺</i> ;;	3.7 \pm 0.2	21	<.0001	
<i>w¹¹¹⁸; dCirl^{KO}; +/20xUAS-dCirl</i> ;	4.8 \pm 0.3	18	<.0001	
<i>w¹¹¹⁸; dCirl^{KO}; iav-GAL4/+</i> ;	4.4 \pm 0.1	22	-	
<i>w¹¹¹⁸; dCirl^{KO}; iav-GAL4/20xUAS-dCirl</i> ;	6.0 \pm 0.4	16	.001	
Related to Figure 5A				
<i>w¹¹¹⁸; dCirl^{KO} w⁻</i> ;;	4.2 \pm 0.3	26	-	-
<i>w[*]; nan^{36a}</i> ;	3.4 \pm 0.3	22	-	.029
<i>w[*]; dCirl^{KO} w⁻; nan^{36a}</i> ;	4.2 \pm 0.1	22	.0183	.893
<i>w[*]; nompC^{f00642..}</i> ;;	5.1 \pm 0.4	17	-	.023
<i>w[*]; dCirl^{KO} w⁻; nompC^{f00642..}</i> ;;	3.8 \pm 0.3	20	.0100	.313
<i>w^{1118...,,,}</i>	6.6 \pm 0.5	19		<.0001
<i>w[*]; dCirl^{KO} w⁻; iav-GAL4/+</i> ;	5.1 \pm 0.3	17	-	
<i>w[*]; dCirl^{KO} w⁻; UAS-nompC::GFP</i> ;;	4.7 \pm 0.2	21	.017	
<i>w[*]; dCirl^{KO} w⁻; UAS-nompC::GFP; iav-GAL4/+</i> ;	6.0 \pm 0.3	25	<.001	

Table S2. Touch sensitivity assay scores. Colors mark independent experimental data sets. Each top entry served as control. Values represent the mean \pm SEM. Related to Figures 2 and S2.

Genotype	TSA score (individual trials) [#]	TSA score (individual larvae = Σ 4 trials) [§]	<i>n</i>	<i>P</i>
Related to Figure 3A				
<i>w[*]; +/Df(2R)Exel8047;;</i>	2.3 \pm 0.1	9.3 \pm 0.5	51	-
<i>w[*]; dCirl^{KO}/Df(2R)Exel8047;;</i>	1.5 \pm 0.1	6.0 \pm 0.5	49	<.0001
<i>w[*]; dCirl^{Rescue}/Df(2R)Exel8047;;</i>	2.0 \pm 0.1	8.0 \pm 0.5	43	.052
<i>w^{1118...,,,}</i>	2.5 \pm 0.1	10.0 \pm 0.7	18	-
<i>w¹¹¹⁸; dCirl^{KO} w⁺;;</i>	1.8 \pm 0.1	7.2 \pm 0.5	18	.007
Related to Figures 3C and S2A				
<i>w^{1118...,,,}</i>	2.9 \pm 0.2	11.4 \pm 0.8	15	-
<i>w¹¹¹⁸; dCirl^{KO} w⁺;;</i>	2.3 \pm 0.2	9.2 \pm 0.6	14	.020
<i>w¹¹¹⁸; dCirl^{KO}; +/20xUAS-dCirl;</i>	1.5 \pm 0.3	6.1 \pm 1.1	12	.002
<i>w¹¹¹⁸; dCirl^{KO} ok6-GAL4/dCirl^{KO}; +;</i>	2.8 \pm 0.2	11.2 \pm 0.7	9	-
<i>w¹¹¹⁸; dCirl^{KO} ok6-GAL4/dCirl^{KO}; 20xUAS-dCirl/+;</i>	2.7 \pm 0.3	10.8 \pm 1.4	10	.869
<i>w¹¹¹⁸; dCirl^{KO} 21-7-GAL4/dCirl^{KO}; +;</i>	3.0 \pm 0.2	12.2 \pm 0.7	11	-
<i>w¹¹¹⁸; dCirl^{KO} 21-7-GAL4/dCirl^{KO}; 20xUAS-dCirl/+;</i>	2.7 \pm 0.3	10.5 \pm 1.0	13	.277
<i>w¹¹¹⁸; dCirl^{KO}; iav-GAL4/+;</i>	2.5 \pm 0.1	9.9 \pm 0.5	14	-
<i>w¹¹¹⁸; dCirl^{KO}; iav-GAL4/20xUAS-dCirl;</i>	3.0 \pm 0.1	11.8 \pm 0.5	18	.019

[#] Value space: 0-4

[§] Value space: 0-16

Table S3. Morphological assessment of *dCirl^{KO}* pentascolopodial organs. Comparison with results by (Caldwell et al., 2003) using a similar scoring system obtained corresponding values for their wild-type control strain *40AG13* for ^amissing scolopidia (1.0-1.9 %), ^bmissing ciliary dilations (6.8-17.0 %) and ^cdefects in relative orientation of the neurons within the pentascolopodial unit (0-6.8 %). Related to Figure 3.

	<i>w⁺; +; iav-GAL4/UAS-20xUAS-IVS-mCD8::GFP;</i>		<i>w⁺; dCirl^{KO}; iav-GAL4/UAS-20xUAS-IVS-mCD8::GFP;</i>		<i>P</i>
	Mean	Percentage	Mean	Percentage	
Scolopidia missing ^a	2	2.5	3	3.75	.653
Ciliary dilation missing ^b	13	16.25	11	13.75	.611
Orientation change ^c	2	2.5	2	2.5	.974
<i>n</i>	80		80		

Table S4. Mechanically triggered action current frequency in *lch5* neurons for initial mutant characterization (A), genomic rescue (B) and chordotonal neuron-specific rescue (C). Note the presence or absence of the *iav-GAL4* driver in the individual datasets. All values represent the mean \pm SEM. f_s = stimulation frequency, f_e = mechanically evoked action current frequency. Related to Figures 3 and S3.

Genotype	(A) Related to Figure 4B			(B) Related to Figure S3B			(C) Related to Figure S3C				
	<i>w⁻; +; iav-GAL4/UAS-20xUAS-IVS-mCD8::GFP;</i>	<i>w⁻; dCirr^{KO}; iav-GAL4/UAS-20xUAS-IVS-mCD8::GFP;</i>	<i>P</i>	<i>w⁻; +; +;</i>	<i>w⁻; dCirr^{Rescue}; +;</i>	<i>P</i>	(1)	(2)	(3)	1 vs 2	1 vs 3
f_s [Hz]	f_e [Hz]	f_e [Hz]	<i>P</i>	f_e [Hz]	f_e [Hz]	<i>P</i>	f_e [Hz]	f_e [Hz]	f_e [Hz]	<i>P</i>	<i>P</i>
0	48 \pm 5	28 \pm 4	.005	28 \pm 5	29 \pm 5	.762	43 \pm 5	34 \pm 5	32 \pm 6	.121	.130
100	65 \pm 9	32 \pm 6	.007	32 \pm 6	33 \pm 5	.880	58 \pm 10	41 \pm 9	36 \pm 9	.199	.221
300	67 \pm 9	34 \pm 6	.016	33 \pm 5	41 \pm 6	.225	60 \pm 10	41 \pm 10	35 \pm 7	.226	.072
500	80 \pm 12	39 \pm 6	.026	36 \pm 5	47 \pm 6	.289	69 \pm 11	40 \pm 10	36 \pm 7	.059	.060
700	88 \pm 12	44 \pm 7	.009	55 \pm 9	59 \pm 7	.496	79 \pm 10	45 \pm 11	44 \pm 7	.041	.013
900	98 \pm 9	45 \pm 8	<.001	78 \pm 11	85 \pm 10	.879	87 \pm 7	45 \pm 11	54 \pm 9	.019	.002
1100	88 \pm 13	40 \pm 6	.010	49 \pm 8	59 \pm 6	.344	72 \pm 9	40 \pm 9	38 \pm 6	.026	.016
1300	79 \pm 11	36 \pm 5	.006	44 \pm 6	54 \pm 6	.212	71 \pm 9	38 \pm 9	35 \pm 6	.014	.013
1500	74 \pm 11	33 \pm 5	.007	41 \pm 7	53 \pm 6	.130	70 \pm 11	37 \pm 9	36 \pm 6	.045	.030
<i>n</i>	10	10		10	10		10	10	9		

Table S5. Startle response score upon stimulation with a 900 Hz tone. Colors mark independent experimental data sets. Each top entry served as control. All values represent the mean \pm SEM. Related to Figure 4.

Genotype	Startle response score at			
	60 dB (n) [P]	70 dB (n) [P]	80 dB (n) [P]	90 dB (n) [P]
<i>w[*]; +/Df(2R)Exel8047;;</i>	.17 \pm .03 (20) -	.57 \pm .06 (20) -	.90 \pm .03 (10) -	.99 \pm .01 (10) -
<i>w[*]; dCirr^{KO}/Df(2R)Exel8047;;</i>	.07 \pm .01 (20) [.005]	.19 \pm .02 (20) [<.0001]	.52 \pm .06 (20) [<.0001]	.91 \pm .02 (20) [.013]
<i>w[*]; dCirr^{Rescue}/Df(2R)Exel8047;;</i>	.15 \pm .04 (10) [.050]	.52 \pm .02 (10) [.611]	.83 \pm .04 (10) [.220]	.98 \pm .01 (10) [.543]
<i>w^{1118...}</i>	.29 \pm .03 (20) -	.58 \pm .03 (20) -	.87 \pm .03 (20) -	.99 \pm .01 (20) -
<i>w¹¹¹⁸; dCirr^{KO} w⁻;;</i>	.10 \pm .03 (20) [<.0001]	.18 \pm .03 (20) [<.0001]	.60 \pm .04 (20) [<.0001]	.87 \pm .02 (20) [<.0001]

Movie S1. *dCirl* is required for locomotion.

Close-up view of single larvae: control, *dCirl*^{KO} and *dCirl*^{Rescue} larvae show extended pausing and head swing phases in *dCirl*-deficient animals. Note that peristaltic contractions of *dCirl*^{KO} are intact.

Groups of larvae: Experimental setup for the measurement of crawling distance. Eight larvae were placed in a petri dish and left to crawl for 2 min. Note the reduced distance travelled by *dCirl*^{KO} larvae and rescue of the phenotype in *dCirl*^{Rescue}.

Related to Figure 2.

SUPPLEMENTAL EXPERIMENTAL PROCEDURES

Fly culture conditions and stocks

Flies and larvae were raised at 25°C on standard cornmeal and molasses medium. The following strains were generated in this study:

- LAT1, $w^{1118}; P\{w^{+mC}=pTL161[dCirl\ targeting\ vector]\};$ (Control)
LAT26, $w^{1118}; dCirl^{KO}\ attP^{dCirl}\ loxP;;$ ($dCirl^{KO}\ w^-$)
LAT54, $w^{1118}; dCirl^{KO}\ attP^{dCirl}\ loxP-w^+-loxP;;$ ($dCirl^{KO}\ w^+$)
LAT79, $w^{1118}; dCirl^{KO}\ \{w^{+mC}=pTL370[dCirl]\}attP^{dCirl}\ loxP;;$ ($dCirl^{Rescue}$)
LAT84, $w^{1118}; dCirl^{KO}\ \{w^{+mC}=pTL464[dCirlp::gal4]\}attP^{dCirl}\ loxP/CyOGFPw^-;;$ ($dCirlp^{GAL4}$)
LAT85, $w^{1118}; \{w^{+mC}=pTL471[20xUAS-IVS-dCirl::3xflag]\}attP^2/TM3, Sb, Kr-GAL4 > UAS-GFP;$ ($20xUAS-dCirl$)
LAT91, $w^{1118}; dCirl^{KO}\ attP^{dCirl}\ loxP\ P\{w^{+mC}=ok6-gal4\}/CyOGFPw^-;;$
GN60, $w^{1118}; P\{w^{+mC}=iav-GAL4\}attP^2;$ (transformation vector was a gift from S. Stowers, Montana State University)

The following strains were obtained from several sources including the Bloomington Stock Center (NIH P40OD018537) and the Harvard Exelixis deficiency collection, or were gifts from colleagues:

- BDSC#766, $y^1\ w^{67c23}\ P\{y^+\ Cre\}^{1b}; sna^{Sco}/CyO;;$
BDSC#851, $y^1\ w^{67c23}\ P\{y^{mDint2}\ Cre\}^{1b}; D^*/TM3\ [Ub^{xbx-34e}\ e^1\ kni^{r-1}\ l(3)89Aa^1\ p^p\ vvl^{sep}], Sb^1;$
BDSC#6938, $w^{1118}; P\{ry^{+t7.2}=70FLP\}^{10};$
BDSC#7863, $w^{1118}; Df(2R)Exel8047/CyO;;$
BDSC#12661, $w^{1118}; P\{w^{+mGT}=GT1\}eys^{BG02208}$ (Bellen et al., 2004; Zelhof et al., 2006);
BDSC#24902, $;;nan^{36a};$ (Kim et al., 2003)
BDSC#25679, $y^1\ w/Dp(2;Y)^G\ P\{w^{+mC}=hs-hid\}^Y;; P\{ry^{+t7.2}=70FLP\}^{23}\ P\{v^{+t1.8}=70I-Scel\}^{4A}/TM3\ P\{w^{+mC}=hs-hid\}^{14}, Sb^1;$
BDSC#26259, $w^-; Pin^1/CyO; P\{?GawB\}^{221};$
BDSC#32194, $w^*;; P\{y^{+t7.7}\ w^{+mC}=20xUAS-IVS-mCD8::GFP\}attP^2;$
BDSC#32197, $w^*;; P\{y^{+t7.7}\ w^{+mC}=10xUAS-IVS-myr::GFP\}attP^2;$
 $w^{1118};$
 $w^*; P\{w^{+mC}=ok6-gal4\};$ (Marqués et al., 2002)
 $w^*; P\{w^{+mC}=UAS-mCD8::GFP\};$
 $w^*; 21-7-GAL4;;$

w^+ ; PBac{WH}nompC^{f00642}/CyO; TM6B, Tb/MKRS, Sb; (Sun et al., 2009)
 w^+ ; P{w^{+mC}= UAS-nompC::GFP};; (Kim et al., 2003)

Transgene construction

pTL161: To generate the *dCirl* targeting construct *pTL161*, first the 3.5 kb 3' homology arm was amplified from BAC clone #BACR21H10 (#RP98-21H10; BacPac repository, Children's Hospital Oakland Research Institute, USA) with primers *tl_53F* and *tl_54R* containing *NsiI* and *AvrII* sites respectively, and inserted into the plasmid *pGX-attP* (Huang et al., 2009). Next, the 5.0 kb 5' homology arm was amplified using primers *tl_51F* and *tl_52R* and also inserted into *pGX-attP-3'arm* plasmid using *NotI* and *KpnI* sites.

pTL370: The *dCirl* rescuing construct was produced by long-range PCR amplification (primers: *tl_299F/tl_300R*) of a 10.8 kb fragment from #BACR21H10. The fragment corresponds exactly to the *dCirl* locus replaced through homologous recombination via the ends-out targeting procedure. The *dCirl* amplicon was inserted into the phiC31-integration vector *pGE-attB-GMR* (Huang et al., 2009) at the *NotI* and *AscI* sites resulting in vector *pTL370*.

pTL464: The transcriptional *dCirl* reporter was constructed by subcloning a 2.1 kb *NotI/MluI*-fragment of *pTL370* into *pMCS5* (resultant clone: *pTL450*). *pTL450* was outward-amplified with primers *tl_420F/421R* *NheI* and *AgeI* sites were introduced between positions -8/-7 to the start methionine in exon 1 (leaving the endogenous Kozak sequence of *dCirl* intact in order to allow unhampered transcription from the *dCirl* locus) and ligated with a 1.6 kb *NheI/AgeI* PCR-fragment amplified from *pBPgal4.2::p65d* with primers *tl_422F/423R* containing an optimized *gal4* cassette (Pfeiffer et al., 2010; resultant clone: *pTL457*). A 3.7 kb *NotI/MluI* fragment from *pTL457* was back-cloned into *pTL370* generating transformation vector *pTL464*.

pTL471: A 7.5 kb *NotI/AgeI dCirl::3xflag* fragment was amplified from *pTL393* with primers *tl_375F/376R* removing the intergenic region 5' of the *dCirl* start methionine containing the *dCirl* promoter and putative enhancer elements. This fragment was inserted into transformation vector *pTL412*, a derivative of *pJFRC7* (Pfeiffer et al., 2010), whose multiple cloning site was extended into *NotI-StuI-KpnI-XhoI-XbaI-3xflag-AgeI*.

All PCR-based cloning steps were performed with AccuStar high-fidelity proof-reading DNA polymerase (Eurogentec). Inserts were first verified by restriction analyses. To ensure absence of errors each PCR-amplified region was completely sequenced. Primer sequences in 5'-3' order, restriction sites in capital letters:

tl_51F: atagtttaGCGGCCGctgtggaatccgcagcactacgacta

tl_52R: cggGGTACCtattgataaatacaaacatatttaact

tl_53F: ccaATGCATtctctgtaagctaagtgctatgca
tl_54R: aatgcaCCTAGGcatcttaacggagctcagagctgt
tl_299F: atagttaGCGGCCGCagtaattgtcttcgatgtatgcat
tl_300R: aGGCGCGCCatttaaagccattttgaaagcaaa
tl_375F: atagttaGCGGCCGCagtatatcccaggcagtgtaaaagcgtatc
tl_376R: taACCGGTtcacttagccagtggtccagataacatcg
tl_420F: ctaGCTAGCgcgtatcatgctaccaacatattg
tl_421R: taACCGGTttttacactgcctgggatatactta
tl_422F: taACCGGTatcaaaatgaagctgctgagtagta
tl_423R: ctaGCTAGCtctagaactagtgatctaaacgag

Ends-out targeting of *dCirl*

We followed the procedures described by (Huang et al., 2008; 2009) and fly strains therein to target the *dCirl* locus (see also Figure S1).

phiC31-mediated recombination into *dCirl^{KO}-attP*

The *w⁺*-marker inserted close to the replaced *dCirl* locus in *dCirl^{KO}* was removed by expression of Cre recombinase according to previous protocols (Huang et al., 2008; 2009). *phiC31[3xP3-RFP-3xP3-GFP-vas-PhiC31]; dCirl^{KO} attP-loxP*; embryos were injected with *w⁺*-marked vectors bestowed with an *attB* site. Recombinants were selected for presence of the *w⁺* marker and precise insertion of the transgene was confirmed by PCR genotyping.

Antibody production

An anti-dCIRL antibody was generated by raising polyclonal serum (BioGenes, Berlin, Germany) against the synthetic peptide corresponding to aa 365-379 of dCIRL (CVLMKRIPDSGYDEY).

Immunohistochemistry and imaging

For immunohistochemical preparations, the following antibody dilutions were used in the study: α -HRP conjugated with Cy3 (1:250; Jan and Jan, 1982), mouse- α -FASII (1D4; 1:25; Lin and Goodman, 1994), mouse- α -GFP (1:500), rabbit- α -GFP (1:500), mouse- α -NOMPC (1:200) (Lee et al., 2010), mouse- α -EYS/SPAM (1:20; Zelhof et al., 2006), Alexa Fluor-488-conjugated goat- α -mouse and goat- α -rabbit (each 1:250; Invitrogen), Cy3-conjugated goat- α -rabbit and goat- α -mouse antibodies (each 1:250; Dianova). Laser power and imaging settings were kept identical for each channel per experiment.

Morphological assessment of L3 pentascolopodial organs

Third instar larvae of the respective genotypes (Control: *w⁺*; *iav-GAL4/UAS-20xUAS-IVS-mCD8::GFP*; *dCirl* mutant: *w⁻*; *dCirl^{KO}*; *iav-GAL4/UAS-20xUAS-IVS-mCD8::GFP*) were dissected and immunostained with an α -GFP antiserum to label *iav-GAL4⁺* neurons, particularly the somatic and ciliary part of the dendrite. Within pentascolopodial organs (lch5) in abdominal segments A2 and A3, individual scolopidia were scored for their presence, and for visibility of their ciliary dilation (Caldwell et al., 2003). In addition, whole lch5 were examined for defects in arrangement of the five neurons with a score for relative orientation.

Immunoblots

Whole flies were collected and homogenized in 2x Laemmli sample buffer on ice. The lysate was subjected to electrophoresis in a 12.5% SDS-PAGE gel and transferred to a polyvinylidene difluoride membranes (Hybond P, Amersham). The membrane was blocked in 5 % milk powder in 1x TBS-T. Blots were probed with either of the following primary antisera at the indicated concentration at 4 °C overnight: rabbit- α -dCIRL (1:500). After washing, membranes were incubated for 1 h at room temperature with HRP-conjugated goat-anti-rabbit (1:2000) or goat-anti-mouse secondary antisera (1:5000; both Sigma-Aldrich), respectively, and washed again according to standard protocols. Western blots were developed by an enhanced chemiluminescence (ECL) detection system.

RT-PCR

Total RNA was isolated from control and *dCirl^{KO}* fly heads using RNeasy RNA Isolation Kit (Qiagen) and was directly used for reverse transcription with Superscript III Reverse Transcriptase (Invitrogen). PCR-amplification on transcribed cDNA libraries was carried out with the following primers:

tl_5F: atgctggtatagatcgagggtgctg

tl_6R: acctgatctataccagcatttacc

tl_444F: gttgcaaccacctgacaaactttgc

Lethal phase analysis

dCirl^{KO}/CyoGFP^w, *dCirl^{KO}/Df* and *+/ CyoGFP^w* larvae were tested for developmental lethality by analyzing their survival rate at 25 °C. Developmental timing across genotypes was synchronized by transferring parental crosses to new vials each day. The number of animals was counted over

16 days post fertilization (d.p.f.) at the following stages: L1 (2 d.p.f.), L3 (7 d.p.f.), pupa (11 d.p.f.) and adult (16 d.p.f.). The experiment was conducted in triplicate and averaged results were normalized to number of L1 animals. Data are displayed as mean \pm SEM.

Electrophysiological analyses

Chordotonal neuron recordings

Male third-instar larvae were pinned on a sylgard block. Preparations of fillets were made in hemolymph-like saline (in mM: 103 NaCl, 3 KCl, 4 MgCl₂, 5 TES, 7 sucrose, 10 glucose, 10 trehalose, 26 NaHCO₃, 1 NaH₂PO₄; pH 7.25)(Zhang et al., 2013). For recording, 2 mM CaCl₂ was added to the saline. Muscles covering the lch5 were gently cut away with fine scissor to expose the organ, then the axon bundle was severed directly after its exit from the lch5. In Figure 4, lch5 neurons were identified by expression of a *20xUAS-IVS-mCD8::GFP* transgene driven by the *iav-GAL4* enhancer in both the control and *dCirr^{KO}* background. Signals were recorded from lch5 neurons by sucking the axon bundle into a recording glass electrode (GB150-8P, Science Products), which was pulled and fire-polished with a DMZ-Universal puller (Zeitz Instruments) to a tip diameter of 5-9 μ m. To apply mechanical stimulation, a fire-sealed glass electrode coupled to a piezo element (KEPO FT-15T-6.0A1-464; Conrad Electronic) was placed at the lch5 cap cells. An upright microscope (Nikon Eclipse-FN-1) equipped with a 40x objective, was used for visualization.

An EPC 10 USB Amplifier (HEKA Instruments) was used for extracellular recordings and to control the piezo device. The stimulation protocol consisted of a series of increasing sine frequencies (100, 300, 500, 700, 900, 1100, 1300, 1500 Hz). For each frequency, three cycles of 1 sec stimulation preceded by 1 sec rest were applied (see also Fig. S6A).

Electrophysiological measurements obtained with Patchmaster (HEKA Instruments) were transferred to Clampfit (Axon Instruments, Molecular Devices) using the ABF Utility software (Synaptosoft). Confirmation of stimulation frequencies was obtained by fast Fourier transform and a notch filter was subsequently used to remove the specific stimulation frequency from recordings. Mechanically-induced action currents of lch5 neurons were detected by template-based search in Clampfit and plotted against vibration frequencies.

Computation of discrimination matrices

All discrimination ratios R_d for each stimulation frequency were computed:

$$R_d = \frac{f_e}{f_b}$$

where f_e is the average evoked response frequency and f_b the average spontaneous (background) spiking frequency of an individual lch5 recording.

We then compared R_d values for each specific stimulation frequency with R_d values for every other stimulation frequency obtained for the same genotype through a nonparametric Mann-Whitney U test. Pairwise comparisons tested the null hypothesis that both samples were identical. The P values for each comparison were color coded and entered into a rectangular array deriving a discrimination matrix for each genotype tested.

Behavioral assays

Touch sensitivity assay

We applied an established touch sensitivity assay (Caldwell et al., 2003; Kernan et al., 1994). Individual larvae were assigned the following score upon gentle touch application: 0, larva not responding to touch. 1, larva stopped or hesitated upon touch. 2, larvae briefly retracted but continued with forward crawling upon touch. 3, larva retracted and turned away from the stimulus $< 90^\circ$ upon touch. 4, larva retracted and turned away $> 90^\circ$ upon touch. Each larva was gently touched during linear locomotion and scored four times. The values were summed up to attain possible scores between 0-16 per individual larva. Genotypes were blinded before scoring.

Sound-induced startle response

Startle response measurements were recorded in a custom-made box housing a 9 cm petri dish filled with a layer of 1 % agarose in H_2O (arena). Behavioral responses of 10-15 L3 larvae were simultaneously digitally recorded in darkness using a webcam (Logitech HD Pro Webcam C920), of which the IR blocking filter was removed. The arena was illuminated with infra-red LEDs. A sine wave tone at a frequency of 900 Hz was generated by a digital encoder (<http://www.wavtones.com/functiongenerator.php>; the sound protocol (1 sec stimulus, 5 sec break; 10 cycles) was implemented using GarageBand 10.0.2 (Apple Inc.) and exported into a digital sound file, which was then played through a computer-connected loudspeaker placed next to the arena in the box. Sound pressure levels were adjusted to 60, 70, 80 and 90 dB SPL, respectively, using a digital sound pressure level measuring device (Voltcraft SL-100; Conrad

Electronics) directly at the arena inside the box. Video recordings were then blinded and shuffled, and the startle responses were evaluated. A larva was scored as responsive when exhibiting startle behavior including pausing, turning and/or backward locomotion, in response to the sound stimulation. The numbers of (A) startled and (B) all animals present in the field of view at a given sound stimulus were counted, and then the fraction of responsive larvae (A/B) was calculated for every sound event.

Phylogenetic analysis

Protein sequences for latrophilin homologs were retrieved with BLAST (Altschul et al., 1997), and the GAIN domain sequence was annotated and extracted based on domain boundaries given in (Arac et al., 2012). Phylogenetic tree analysis was performed on this GAIN domain sequence set with software packages contained in the software Geneious R6 (Biomatters Ltd.) using the Blosom62 substitution matrix and a neighbor-joining algorithm (gap open penalty = 12, gap extension penalty = 3, Jukes-Cantor genetic distance model).

Determination of putative RFX and Fd3F binding sites in the *dCirl* promoter

The 2.2 kb intergenic region upstream of the start ATG in exon 1 of the *dCirl* open reading frame containing the putative promoter region of the gene was subjected to a search for several RFX consensus sites of increasing stringency as previously defined (Emery et al., 1996; Gajiwala et al., 2000; Laurençon et al., 2007) (Figure S7). The forkhead transcription factor consensus site RYMAAYA used to search for a Fd3F binding site in the *dCirl* promoter fragment was reported in (Benayoun et al., 2008). For the alignment of 12 *Drosophila* genomes the *dCirl* promoter region containing the RFX and Fd3F binding sites (coordinates: chr2R:4,503,445-4,503,519) were displayed and exported from the UCSC genome browser (Kent et al., 2002) using the *D. melanogaster* genome assembly Apr. 2006-BDGP R5/dm3.

SUPPLEMENTAL REFERENCES

Altschul, S.F., Madden, T.L., Schäffer, A.A., Zhang, J., Zhang, Z., Miller, W., and Lipman, D.J. (1997). Gapped BLAST and PSI-BLAST: a new generation of protein database search programs. *Nucleic Acids Res.* *25*, 3389–3402.

Araç, D., Boucard, A.A., Bolliger, M.F., Nguyen, J., Soltis, S.M., Südhof, T.C., and Brunger, A.T. (2012). A novel evolutionarily conserved domain of cell-adhesion GPCRs mediates autoproteolysis. *EMBO J.* *31*, 1364–1378.

Bellen, H.J., Levis, R.W., Liao, G., He, Y., Carlson, J.W., Tsang, G., Evans-Holm, M., Hiesinger, P.R., Schulze, K.L., Rubin, G.M., et al. (2004). The BDGP gene disruption project: single transposon insertions associated with 40% of *Drosophila* genes. *Genetics* *167*, 761–781.

Benayoun, B.A., Caburet, S., Dipietromaria, A., Bailly-Bechet, M., Batista, F., Fellous, M., Vaiman, D., and Veitia, R.A. (2008). The identification and characterization of a FOXL2 response element provides insights into the pathogenesis of mutant alleles. *Hum. Mol. Genet.* *17*, 3118–3127.

Caldwell, J.C., Miller, M.M., Wing, S., Soll, D.R., and Eberl, D.F. (2003). Dynamic analysis of larval locomotion in *Drosophila* chordotonal organ mutants. *Proc. Natl. Acad. Sci. USA* *100*, 16053–16058.

Drosophila 12 Genomes Consortium, Clark, A.G., Eisen, M.B., Smith, D.R., Bergman, C.M., Oliver, B., Markow, T.A., Kaufman, T.C., Kellis, M., Gelbart, W., et al. (2007). Evolution of genes and genomes on the *Drosophila* phylogeny. *Nature* *450*, 203–218.

Emery, P., Strubin, M., Hofmann, K., Bucher, P., Mach, B., and Reith, W. (1996). A consensus motif in the RFX DNA binding domain and binding domain mutants with altered specificity. *Mol. Cell. Biol.* *16*, 4486–4494.

Gajiwala, K.S., Chen, H., Cornille, F., Roques, B.P., Reith, W., Mach, B., and Burley, S.K. (2000). Structure of the winged-helix protein hRFX1 reveals a new mode of DNA binding. *Nature* *403*, 916–921.

Huang, J., Zhou, W., Dong, W., Watson, A.M., and Hong, Y. (2009). Directed, efficient, and versatile modifications of the *Drosophila* genome by genomic engineering. *Proc. Natl. Acad. Sci. USA* *106*, 8284–8289.

Huang, J., Zhou, W., Watson, A.M., Jan, Y.-N., and Hong, Y. (2008). Efficient ends-out gene targeting in *Drosophila*. *Genetics* *180*, 703–707.

Jan, L.Y., and Jan, Y.N. (1982). Antibodies to horseradish peroxidase as specific neuronal markers in *Drosophila* and in grasshopper embryos. *Proc. Natl. Acad. Sci. USA* *79*, 2700–2704.

Kent, W.J., Sugnet, C.W., Furey, T.S., Roskin, K.M., Pringle, T.H., Zahler, A.M., and Haussler, D. (2002). The human genome browser at UCSC. *Genome Res.* *12*, 996–1006.

Kernan, M., Cowan, D., and Zuker, C. (1994). Genetic dissection of mechanosensory transduction: mechanoreception-defective mutations of *Drosophila*. *Neuron* *12*, 1195–1206.

Kim, J., Chung, Y.D., Park, D.-Y., Choi, S., Shin, D.W., Soh, H., Lee, H.W., Son, W., Yim, J., Park, C.-S., et al. (2003). A TRPV family ion channel required for hearing in *Drosophila*. *Nature* *424*, 81–84.

Laurençon, A., Dubruille, R., Efimenko, E., Grenier, G., Bissett, R., Cortier, E., Rolland, V., Swoboda, P., and Durand, B. (2007). Identification of novel regulatory factor X (RFX) target genes by comparative genomics in *Drosophila* species. *Genome Biol.* *8*, R195.

Lee, J., Moon, S., Cha, Y., and Chung, Y.D. (2010). *Drosophila* TRPN(=NOMPC) channel localizes to the distal end of mechanosensory cilia. *PLoS ONE* *5*, e11012.

Lin, D.M., and Goodman, C.S. (1994). Ectopic and increased expression of Fasciclin II alters motoneuron growth cone guidance. *Neuron* *13*, 507–523.

Marqués, G., Bao, H., Haerry, T.E., Shimell, M.J., Duchek, P., Zhang, B., and O'Connor, M.B. (2002). The *Drosophila* BMP type II receptor Wishful Thinking regulates neuromuscular synapse morphology and function. *Neuron* *33*, 529–543.

Pfeiffer, B.D., Ngo, T.T.B., Hibbard, K.L., Murphy, C., Jenett, A., Truman, J.W., and Rubin, G.M. (2010). Refinement of Tools for Targeted Gene Expression in *Drosophila*. *Genetics* *186*, 735–755.

Sun, Y., Liu, L., Ben-Shahar, Y., Jacobs, J.S., Eberl, D.F., and Welsh, M.J. (2009). TRPA channels distinguish gravity sensing from hearing in Johnston's organ. *Proc. Natl. Acad. Sci. U S A* *106*, 13606–13611.

Zelhof, A.C., Hardy, R.W., Becker, A., and Zuker, C.S. (2006). Transforming the architecture of compound eyes. *Nature* *443*, 696–699.

Zhang, W., Yan, Z., Jan, L.Y., and Jan, Y.-N. (2013). Sound response mediated by the TRP channels NOMPC, NANCHUNG, and INACTIVE in chordotonal organs of *Drosophila* larvae. *Proc. Natl. Acad. Sci. USA* *110*, 13612–13617.